

Melting and Crustal Processes at the FAMOUS Segment (Mid-Atlantic Ridge): New Insights from Olivine-hosted Melt Inclusions from Multiple Samples

MURIEL LAUBIER*, ALLISON GALE AND CHARLES H. LANGMUIR

DEPARTMENT OF EARTH AND PLANETARY SCIENCES, HARVARD UNIVERSITY, 20 OXFORD STREET, CAMBRIDGE, MA 02138, USA

RECEIVED SEPTEMBER 29, 2010; ACCEPTED DECEMBER 2, 2011

Most published studies of olivine-hosted melt inclusions from mid-ocean ridges have been based on a single sample. Here we present a comprehensive melt inclusion study of major and trace elements from a single ocean ridge segment, the FAMOUS segment of the Mid-Atlantic Ridge. The melt inclusion dataset includes 312 olivine-hosted (Mg-number 85–92) melt inclusions from 14 samples distributed along the segment. This permits a more comprehensive assessment of the variability within melt inclusions from a single region, and of the relationship between melt inclusion and lava compositions. One recent question has been the extent to which melt inclusions truly preserve the original melt compositions, or instead are modified by late-stage processes occurring at shallow levels. In the FAMOUS inclusions, major elements have been affected by post-entrapment processes, but trace elements show no evidence of such processes, suggesting that diffusion coefficients for incompatible elements are small. Melt inclusions can be divided into three groups. (1) High-Mg inclusions are the most primitive and may potentially constrain the composition of the parental magmas that contribute to other melt inclusion and lava compositions. Although their trace element contents range from highly depleted to almost as enriched as the FAMOUS segment lavas, they are on average more depleted and the melts appear to be derived by greater extents of melting than the lavas. (2) Low-Al inclusions occur in the lower Mg-number olivines, and their major and trace element characteristics reflect mixing between high-Mg melt inclusion and lava compositions. (3) High-Al melt inclusions display Al_2O_3 contents as high as 18.4 wt %, SiO_2 as low as 46.6 wt %, a strong depletion in the most incompatible elements and distinctively low middle to heavy rare earth element

(MREE/HREE) ratios. The high Al_2O_3 and low SiO_2 contents, as well as positive Sr anomalies in some of the high-Al melt inclusions, are best explained by assimilation of plagioclase-bearing cumulates. The trace element variability in the high-Mg melt inclusions is not consistent with a simple continuous melting column and requires pooling of near-fractional melts within the melting regime and a variable mantle source composition. Because the mean composition of these melt inclusions reflects greater extents of melting than the lavas, we propose that the melt inclusions come from the upper portions of the melting regime. Lavas, in contrast, sample the entire melting regime, including low-degree melts from the wings of the regime that are transported more directly to the surface along high-porosity channels. The high-Al, trace element ultra-depleted, low MREE/HREE melt inclusions derive from melting of a residual mantle source formed by previous melt extraction in the garnet stability field. There is a marked lack of correspondence between major and trace element variations in the melt inclusions. This may reflect a combination of processes, such as cumulate assimilation and re-equilibration of the magmas during ascent, which can reset major elements while having little effect on the trace element variations. The melt inclusions are not simply representative unpooled melts from the melting regime and they do not fully reflect the range of melt compositions contributing to the lavas. Their compositions reflect source heterogeneity as well as melting processes, and major and trace element indicators of depth of origin do not correspond. Combined comprehensive studies of lavas and melt inclusions have much more to reveal than studies based on either data source alone.

*Corresponding author. Telephone: +1-617-496-6924. Fax: +1-617-496-6958. E-mail: laubier@eps.harvard.edu

KEY WORDS: *melt inclusion; mid-ocean ridge; olivine; partial melting*

INTRODUCTION

Understanding petrogenetic processes encounters the difficulty that magmas erupted at the surface are not the primitive magmas derived directly from the mantle. One promising approach towards alleviating this problem has been the study of melt inclusions in minerals. Melt inclusions are trapped in minerals at an earlier stage of magma genesis than that at which the lava is erupted, and the host mineral isolates them from subsequent magmatic processes. Thus, melt inclusions in principle record a more primitive stage of petrogenesis than the erupted lava, and may provide a history of the processes that have occurred. This great potential of melt inclusions has long been recognized, and work by Sobolev & Kostyuk (1975), Roedder (1979), Lowenstern (1995), Sobolev (1996), Frezzotti (2001), Schiano (2003) and Kent (2008) has led the way to using melt inclusions as petrogenetic tools.

On mid-ocean ridges, particularly influential work was carried out by Sobolev & Shimizu (1993), in which they identified an ultra-depleted melt inclusion and used it to infer that fractional melts of the mantle could be preserved as melt inclusions. Gurenko & Chaussidon (1995) and Sobolev (1996) then used a suite of melt inclusions to infer fractional melting during polybaric upwelling by showing that depleted melt inclusions were apparently formed at the shallowest depth in the mantle. The concept that arises from this melt inclusion work is that an array of primary melts is generated in the mantle; these melts then mix together to form the parental magmas that subsequently fractionate at various pressures to generate the magmas that are erupted at the surface. This conclusion was previously inferred from the chemical compositions of ocean ridge basalts (Klein & Langmuir, 1987; Langmuir *et al.*, 1992).

Very unusual melt inclusion compositions are frequently reported, however, that do not conform to this picture. Large positive Sr anomalies or high Ca contents, for example (Kamenetsky *et al.*, 1998; Slater *et al.*, 2001; Danyushevsky *et al.*, 2003, 2004), have been ascribed to localized assimilation of plagioclase-rich assemblages. Van Orman *et al.* (2002) attributed the extreme depletion in some melt inclusions to re-equilibration of the melts with depleted peridotite during percolation through a low-porosity network, rather than to mantle melting column effects.

This diversity of results and interpretations can be formulated as two competing hypotheses to account for the wide variability found in olivine-hosted melt inclusions in mid-ocean ridge basalt (MORB) (Sobolev & Shimizu, 1993; Sobolev & Nikogosian, 1994; Gurenko & Chaussidon, 1995; Kamenetsky, 1996; Sobolev, 1996; Kamenetsky & Crawford, 1998; Shimizu, 1998; Sobolev

et al., 2000; Slater *et al.*, 2001; Danyushevsky *et al.*, 2002a; Norman *et al.*, 2002; Sours-Page *et al.*, 2002; Font *et al.*, 2007; Kamenetsky & Gurenko, 2007; Laubier *et al.*, 2007; Shaw *et al.*, 2010). The first interprets the melt inclusions as the products of mantle source heterogeneity, partial melting, melt extraction and transport. Mantle source heterogeneity is required to explain the characteristics of melt inclusions from Iceland, for example, that show Pb isotope compositions strongly correlated with trace element compositions (MacLennan, 2008b), and from different oceanic island localities (Saal *et al.*, 1998, 2005; Kobayashi *et al.*, 2004; Yurimoto *et al.*, 2004; Jackson & Hart, 2006). The second hypothesis calls on reactions between peridotitic or crustal lithologies and migrating melts (Kamenetsky & Crawford, 1998; Danyushevsky *et al.*, 2003, 2004). This latter hypothesis implies that many melt inclusions cannot be considered reliable petrogenetic indicators to broaden our understanding of mantle partial melting processes, source heterogeneity and melt extraction processes.

Another factor that can influence the compositions of olivine-hosted melt inclusions is post-entrapment diffusion, a process that is particularly important for fast-diffusing species such as Fe and Mg (Danyushevsky *et al.*, 2000; Gaetani & Watson, 2000, 2002). Some recent results on the diffusion of the rare earth elements (REE) (Spandler *et al.*, 2007) suggest that even for trace elements post-entrapment re-equilibration may be far more extensive than previously assumed. This has been widely recognized for plagioclase-hosted melt inclusions (e.g. Cottrell *et al.*, 2002) but was assumed to be negligible for olivine-hosted inclusions. If the Spandler *et al.* (2007) results are correct, then virtually all melt inclusions may have been modified by re-equilibration processes. These results are, however, inconsistent with more recent data for REE diffusion in olivine by Cherniak (2010). Diffusive effects, therefore, remain an unresolved problem that needs to be considered.

One of the characteristics of most previous work on olivine-hosted melt inclusions in MORB is the lack of representative sampling or a regional perspective. Many of the influential papers are based on inclusions found within a single olivine-rich sample, studied without consideration of the variations in the lavas in the region, or to what extent the sample may or not be representative (e.g. Sobolev & Shimizu, 1993; Kamenetsky, 1996; Sobolev, 1996; Kamenetsky & Crawford, 1998; Kamenetsky *et al.*, 1998; Shimizu, 1998; Danyushevsky *et al.*, 2003; Kamenetsky & Gurenko, 2007; Laubier *et al.*, 2007). The study by Sours-Page *et al.* (1999, 2002) is an exception, but many of their data are for plagioclase-hosted melt inclusions, which have other problems of interpretation. The novel aspect of the present study is that it presents a large set of major and trace element data for multiple (14) samples from the same ridge segment, coupled with an intensive sampling and analysis of the lavas within the same

segment (Gale *et al.*, 2009, and in preparation). Our approach allows certain new questions to be addressed, such as the following. To what extent do regional variations in melt inclusions exist? Are there variations within a ridge segment that may correlate with position in the segment? How well do major and trace elements in inclusions correlate, and how do these variations compare with similar data on lavas from the same region? Is the average melt inclusion a suitable parent for the lava compositions? The large number of melt inclusions, spatial coverage and coupled major and trace element investigation of the same set of inclusions permit a more robust evaluation of the utility and difficulties of interpretation of MORB melt inclusion data.

FIELD AREA AND SAMPLE SELECTION

Our study focuses on the FAMOUS segment near 36°47'N on the Mid-Atlantic Ridge because it is exceptionally well sampled and has a high proportion of relatively primitive lavas and high forsterite olivine-phyric samples, suggesting minimal modification from mantle-derived melts. The segment is 45 km long, and is bounded on the north and south by 25 km offsets from the adjacent AMAR segment to the south and the North Famous segment to the north (Fig. 1). The volcanic morphology of the FAMOUS segment is marked by small volcanic centers located on the floor of the rift valley, and no clearly defined axial volcanic ridge. There is an extensive lava dataset and a rich history of petrogenetic interpretation in terms of mantle processes and source composition (e.g. Bougault, 1977; Bryan & Moore, 1977; Langmuir *et al.*, 1977; Le Roex *et al.*, 1981; Stakes *et al.*, 1984). Basalts from the FAMOUS segment were used as the basis of the dynamic melting concept, because of the large variations in trace element composition in high-Mg samples (Langmuir *et al.*, 1977) with no recognizable variations in radiogenic isotope compositions based on the analytical precision at that time. Subsequent work has shown that major element compositions from this segment have a very well-developed 'local vector', which has been ascribed to melting column effects (Asimow *et al.*, 2004; Langmuir *et al.*, 1992). Therefore, there is evidence in the lavas of a similar mantle melting column signal to that which Sobolev (1996) inferred from the melt inclusion data from a single sample elsewhere on the Mid-Atlantic Ridge.

Fourteen samples from the FAMOUS segment were selected for this melt inclusion study, to encompass a range of compositions and positions within the segment. Indeed, melt inclusions were analyzed in some of the most depleted lavas found at FAMOUS (e.g. ALV527-1) and in the most enriched lava, a true E-MORB (NR-DR-3-4). The sample locations are shown in Fig. 1 and sample information is

presented in Electronic Appendix 1 (downloadable from <http://www.petrology.oxfordjournals.org/>). The samples all contain primitive euhedral olivine phenocrysts that display a range of Mg-number [= 100MgO/(MgO + FeO*), where FeO* corresponds to total iron reported as Fe²⁺], from 85 to 92. Samples ARP73-10-03 and CH31-DR8 are picrites containing more than 20% olivine phenocrysts (1–5 mm), which result from mechanical accumulation of olivine. The remaining samples are olivine-phyric lavas containing euhedral olivine phenocrysts, and also some resorbed megacrystic olivine.

Primary glass inclusions in the olivine crystals are sub-spherical (10–300 µm in diameter). They contain no daughter minerals and relatively rare shrinkage bubbles, consistent with fast cooling by quenching of the crystals. Cr-spinels are frequent inclusions in the olivine crystals and are sometimes trapped in the melt inclusions, as they probably aided melt entrapment in the olivine.

To have a consistent dataset and to be able to make detailed comparison with basalt variations within the segment, 150 basaltic glasses from both the French and US cruises were selected all along the segment and analyzed for their major and trace element, and Sr, Nd and Pb isotope compositions. These data and their interpretation will be published in a separate paper (Gale *et al.*, in preparation).

ANALYTICAL TECHNIQUES

Electron microprobe analysis

Major element compositions of melt inclusions and host olivine crystals were measured with a Cameca SX-100 at Rensselaer Polytechnic Institute (Troy, NY) and a Cameca SX-50 at UMass (Amherst, MA). The following routine was used for glass: an accelerating voltage of 15 kV, a sample current of 10 nA for Na (20 s), Fe (40 s), Si (20 s), Al (20 s) and Ca (40 s), and 50 nA for Mg (50 s), Ti (50 s), K (60 s), Cr (50 s), Mn (50 s), P (50 s), S (50 s) and Cl (70 s), and a defocused beam of 10 µm. For the olivines, we used a beam size of 1 µm and a beam current of 100 nA for Si (30 s), Mg (40 s), Al (40–70 s), Ca (60 s), Fe (40–60 s), Mn (40 s), Ni (40 s) and Cr (40–60 s). The Cameca set of standards (synthetic and natural minerals or oxides) was used for routine calibration, except for Al in glass, which was calibrated on the USGS VG-2 glass standard (Thornber *et al.*, 2002). Analytical uncertainties were obtained from replicate measurements on the natural glasses USGS VG-2 (Dixon *et al.*, 1991; Thordarson *et al.*, 1996; de Hoog *et al.*, 2001; Thornber *et al.*, 2002), USGS A99 (Dixon *et al.*, 1991; Thordarson *et al.*, 1996; de Hoog *et al.*, 2001; Thornber *et al.*, 2002), our in-house standard VE32 and USNM 113716 (Thornber *et al.*, 2002). The total analytical 2σ error, which corresponds to the maximum value between the precision and accuracy of measurements, for the VG-2 basaltic glass was 2.1% rel.

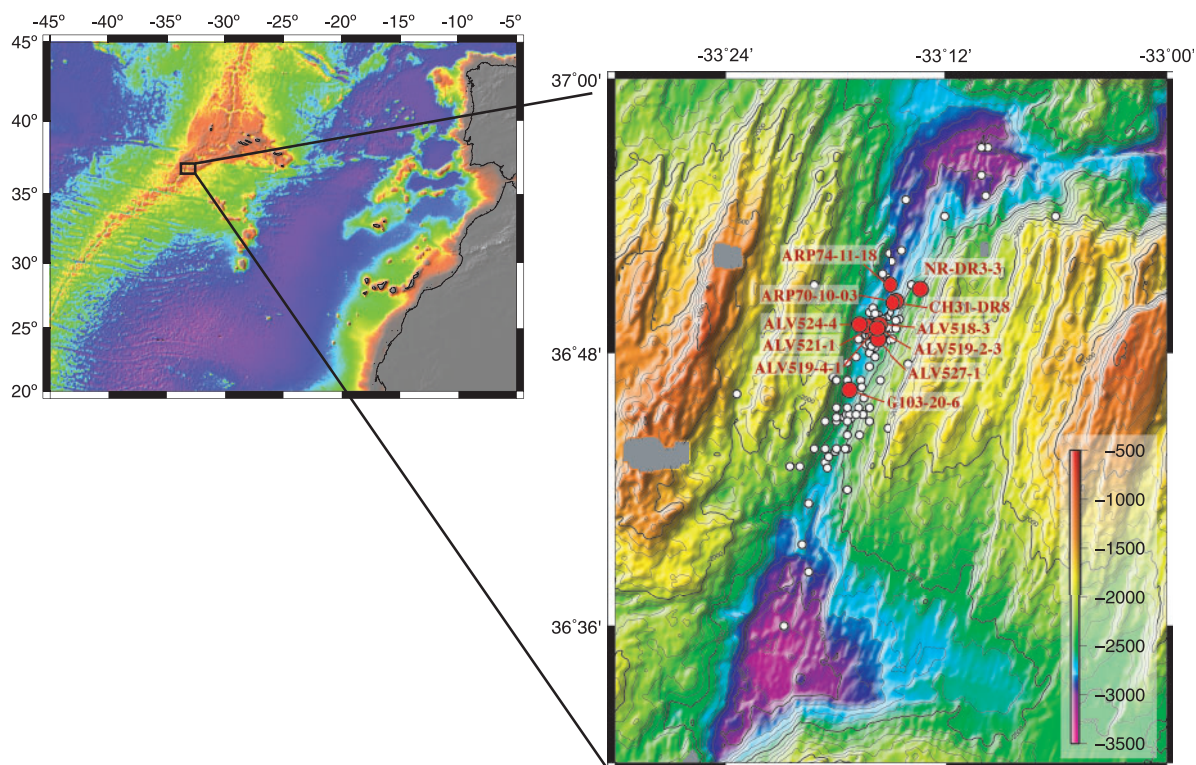


Fig. 1. Bathymetric map of the FAMOUS area, Mid-Atlantic Ridge, showing the location of the melt inclusion samples (filled circles) and glass samples (open circles) used in this study and by Gale *et al.* (in preparation). Global multi-resolution bathymetry as compiled by Ryan *et al.* (2009) was used for the regional map (bathymetry in meters below sea level).

for SiO₂; 1.8% for MgO, TiO₂ and Al₂O₃; 2.4% for CaO; 2.7% for K₂O; 3.4% for FeO; 7–8 % for Na₂O and P₂O₅; 12% for MnO; and 30% for Cr₂O₃. Detection limits for S and Cl were ~ 80 and 90 ppm respectively and the total analytical 2σ error for S and Cl, including precision and accuracy of measurements, was 15% rel. for S and 40% rel. for Cl for the concentrations analyzed in our inclusions. The internal glass standard VE32 was repeatedly analyzed during the runs to monitor instrumental drift over time. Single analyses reported in Electronic Appendix 2 are normalized to the VE32 standard, for which values are also reported.

No effect of alkali loss was observed on natural glasses of basaltic composition (ALV 981 R23, VG-2, VG-A99 and VE32) under the analytical conditions applied during melt inclusion analysis: 15 kV, 10 nA and a 10 μm beam. This effect exists under these conditions for Si-rich glasses only (e.g. in the following glass standards: pantellerite Kel2 from Kenya, Metrich & Rutherford, 1992; subalkaline rhyolite ATHO from Iceland, Oskarsson *et al.*, 1982).

Laser ICP-MS

Trace element compositions of the melt inclusions and host olivines were measured by laser ablation inductively coupled plasma mass spectrometry (LA-ICP-MS) using a

Thermoelectron X-Series ICP-MS system coupled with a pulsed 213 nm ArF Excimer laser (New Wave/Merchantek) at Harvard University. The laser ablation aerosol is carried to the ICP-MS system by a He carrier gas. Argon is used for the nebulizer gas flow, the auxiliary gas flow and the cooling gas flow. Cross-calibrated pulse counting and analog detection (dual-detector mode) in peak-hopping mode allows the measurement of major and trace elements from a single ablation. The repetition rate on the laser is 10 Hz and the beam diameter ranges between 40 and 55 μm. The dwell time per isotope is 10 ms. The total acquisition time is 180 s with an ablation time of 60–80 s, a starting 40 s and an ending 80 s count on the gas blank. In every run, four of the following glass standards (VE32, BHVO-2G, BIR-2, in-house standard MAR and EN026 10D-3, a MORB standard from Jean-Guy Schilling, University of Rhode Island, USA) are used as calibration standards. These standards have been well characterized by solution ICP-MS measurements. They were analyzed three times, evenly spaced in time, during the experiment, with two standards analyzed every 3–4 samples. One standard (VE32 or VG-2) was also analyzed as an unknown sample (see Electronic Appendix 2). The analytical setup is tuned for optimum performance across the entire mass range before every run, to improve the

detection limits for each element. The concentration of calcium, previously determined by electron microprobe with an error of 2.4% rel. (2σ), is used as an internal standard (or normalizing element) during the analysis of melt inclusions. The maximum values for the accuracy and precision of the trace element measurements given by repeated analyses of the glass standards ($n = 57\text{--}106$ per standard) and several melt inclusions ($n = 3$ per melt inclusion) in different runs are $\leq 10\%$ (2σ) for most elements, 12% for Sc, $\leq 15\%$ for Rb, Th, middle REE (MREE) and heavy REE (HREE), 16% for Zn, 30% for U.

Although previously published ion probe data (Shimizu, 1998; Laubier *et al.*, 2007) and LA-ICP-MS analyses on FAMOUS melt inclusions generally agree, discrepancies exist for Y, Eu and Sr (see Electronic Appendix 3). Laser and solution ICP-MS data are, however, extremely consistent between melt inclusions and lavas, and also between *in situ* analyses and solution analyses on the same lava samples. We therefore removed the concentrations of Y, Sr and Eu data from previously published datasets of FAMOUS melt inclusions that were collected on ion probes.

RESULTS

A total of 312 melt inclusions were analyzed and used in the following discussion. In total, 188 new melt inclusions and their host minerals were analyzed for major elements (raw data and data corrected for post-entrapment modification are reported in Electronic Appendix 2). We also include data for 95 olivine-hosted melt inclusions from Laubier *et al.* (2007), nine spinel-hosted melt inclusions from sample ARP73-10-03 (Kamenetsky, 1996) and 20 olivine-hosted melt inclusions from Shimizu (1998) from the sample ALV519-4-1. The Mg-numbers of the host olivine crystals range between 85.3 and 92.2.

Melt inclusion–olivine equilibrium and post-entrapment re-equilibration

Post-entrapment modifications must be accounted for if melt inclusions are to provide petrogenetic information. Such modifications can occur by crystal growth during cooling and by diffusive exchange with the host mineral or the surrounding melt.

During cooling, olivine crystallizes onto the inclusion wall, lowering the Mg content and Mg-number of the melt inclusion. Other daughter minerals can also occasionally form. Because the FAMOUS melt inclusions show no daughter minerals other than olivine, late-stage crystallization can be corrected for by adding olivine back into the melt until its composition is in equilibrium with the olivine host. This correction is adequate as long as there has not been significant diffusive exchange within the mineral or with the host magma.

The extent to which diffusive exchange modifies melt inclusion compositions depends on the diffusivity of the

species in the host crystal, the size of the inclusion and its host, and the partition coefficients of the different elements (Qin *et al.*, 1992). Small inclusions, high diffusivities and high concentrations in the host mineral all enhance the likelihood of exchange effects. Fe and Mg have both high concentrations and high diffusivities, and several studies have demonstrated that Fe^{2+}/Mg inter-diffusion between olivine and basaltic melt can be significant at typical magmatic temperatures (Danyushevsky *et al.*, 2000; Gaetani & Watson, 2000, 2002).

Danyushevsky and co-workers (Danyushevsky *et al.*, 2000, 2002) in particular have emphasized the substantial effects of Fe/Mg diffusion on the compositions of melt inclusions. For example, if an inclusion forms at 1300°C and cools to 1200°C, then significant olivine will have crystallized on the inclusion walls. If the mineral is maintained at 1200°C, diffusion will re-equilibrate the inclusion with the large mass of host olivine (which formed at 1300°C). This would lead to an inclusion with a much lower FeO content, and yet an Mg-number in equilibrium with the host. Further olivine crystallization would lead to a low Mg-number inclusion, and correction back to the host would lead to the modified 1200°C inclusion, not the original 1300°C inclusion. The result is a ‘low-Fe’ inclusion, and indeed, FeO contents of many primitive melt inclusions are lower than the compositions predicted by the liquid lines of descent (LLDs) followed by the lavas (Danyushevsky *et al.*, 2000, 2002a,b). This effect also affects the abundances of other elements, because the total mass of liquid in the inclusion is less than when it was originally captured.

Diffusive effects could also be important for other elements if diffusion coefficients are high. Spandler *et al.* (2007) suggested the diffusion coefficients for the REE might be as high as for Fe and Mg, raising the possibility that incompatible trace elements might also be subject to diffusive exchange. More recent measurements of diffusion of REE in Mg-rich olivine (Cherniak, 2010; Spandler & O’Neill, 2010) are two to three orders of magnitude slower, however, which would lead to minimal exchange. We address this issue for trace elements further below, after presentation of the trace element data. Here we turn to the question of whether useful information can still be obtained from the FeO contents of melt inclusions.

First, we used the reverse crystallization program in the Petrolog package (Danyushevsky & Plechov, 2011) and corrected each melt inclusion composition to be in equilibrium with its host olivine using the model of Toplis (2005) for the equilibrium value of $K_{\text{D.Liq/Ol}}^{\text{Fe/Mg}}$. We assume a pressure of crystallization of 1 bar and an oxygen fugacity of QFM (quartz–fayalite–magnetite). The amount of post-entrapment olivine crystallization derived from the calculation is used to correct the trace-element compositions, using the following partition coefficients:

$D_{Sc} = 0.25$, $D_V = 0.08$, $D_{Cr} = 0.3$, $D_{Co} = 4.5$, $D_{Ni} = 20$, $D_{Cu} = 0.1$, $D_{Zn} = 0.8$ and a value of zero for all the other elements (i.e. assumed to be perfectly incompatible). We then corrected both lavas and melt inclusions back to equilibrium with Fo₉₀ olivine to have a common basis for comparison.

Melt inclusion and lava compositions corrected in this way are illustrated in Fig. 2. The high-Fe end of the inclusion data corresponds to the lavas, but the inclusions range to significantly lower FeO contents (6.3% vs 8%). This deviation toward lower FeO contents is indicative of some Fe loss, which must be corrected for. The continuous-line arrows in Fig. 2 show the trends for correction for diffusive re-equilibration (using the Fe-loss correction program in the Petrolog package; Danyushevsky & Plechov, 2011). As the correction slopes roughly correspond to the overall trend of the data, estimates of the amount of correction are problematic. Regardless of the exact

amount of the re-equilibration correction, however, there are key features in the melt inclusion dataset that will remain. For example, the larger chemical range seen in the inclusions compared with the lavas, and their extension to higher Ca₉₀ and Al₉₀ and lower Si₉₀, are robust features of the melt inclusion data (Fig. 2a–c).

Danyushevsky *et al.* (2000) generally corrected all melt inclusions to a constant FeO value, but this approach eliminates any real FeO variations that may have existed in the melt inclusion dataset. A significant range in FeO contents exists in the lavas, so correcting the melt inclusion data to a constant FeO content would eliminate real variations (Fig. 2). The question then becomes whether there is some other aspect of the data that could be used to estimate an appropriate FeO content for melt inclusions that have undergone Fe loss.

An approach that is promising makes use of the trace element data. Because the trace element abundances

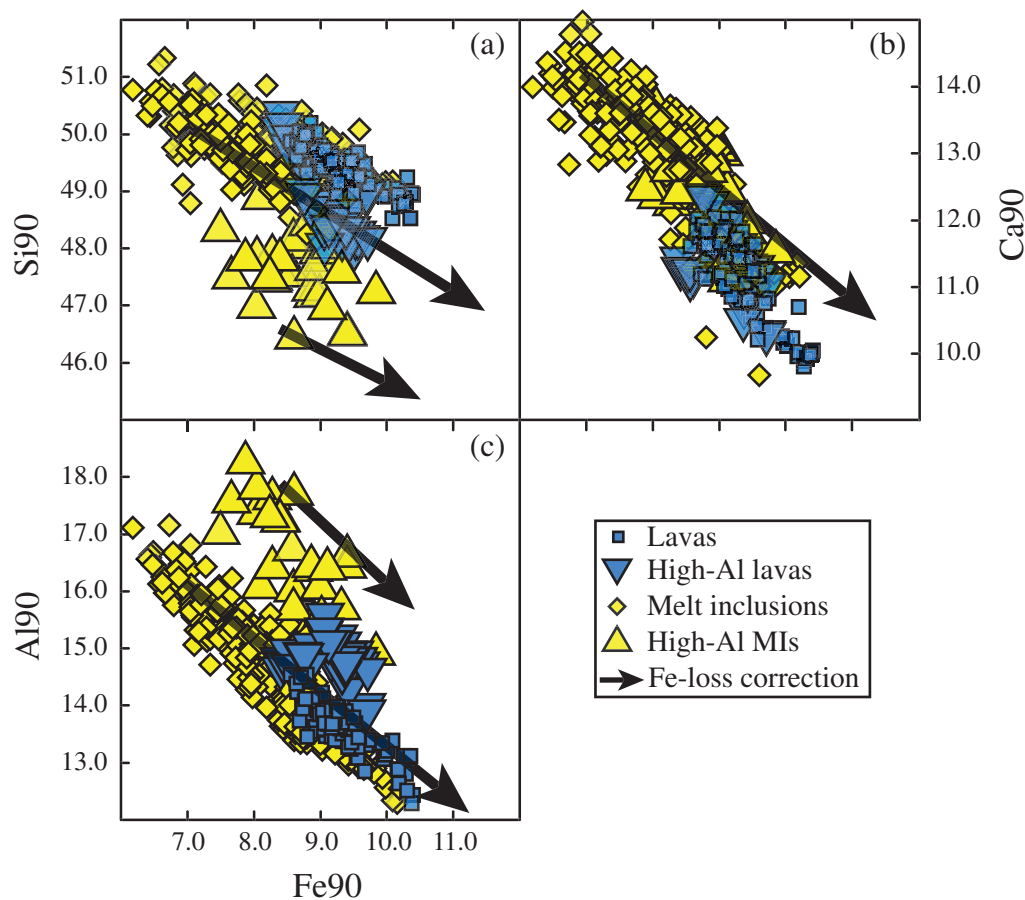


Fig. 2. Melt inclusion and lava compositions in equilibrium with Fo₉₀ olivine. The ‘reverse crystallization’ option of Petrolog (see text for details) was used to correct the melt inclusion data for olivine overgrowth at the inclusion walls (referred to as ‘normal’ correction in the text). In the lavas, plag + cpx + ol fractionation was corrected for manually using a single slope as the slope created by Petrolog was inconsistent with that of the data; olivine fractionation was corrected for using Petrolog. The arrows show the trajectory of the correction for Fe–Mg diffusion between the melt inclusions and the host olivine, as the assumed initial FeO content in the melt inclusion increases (see text and Danyushevsky *et al.*, 2000).

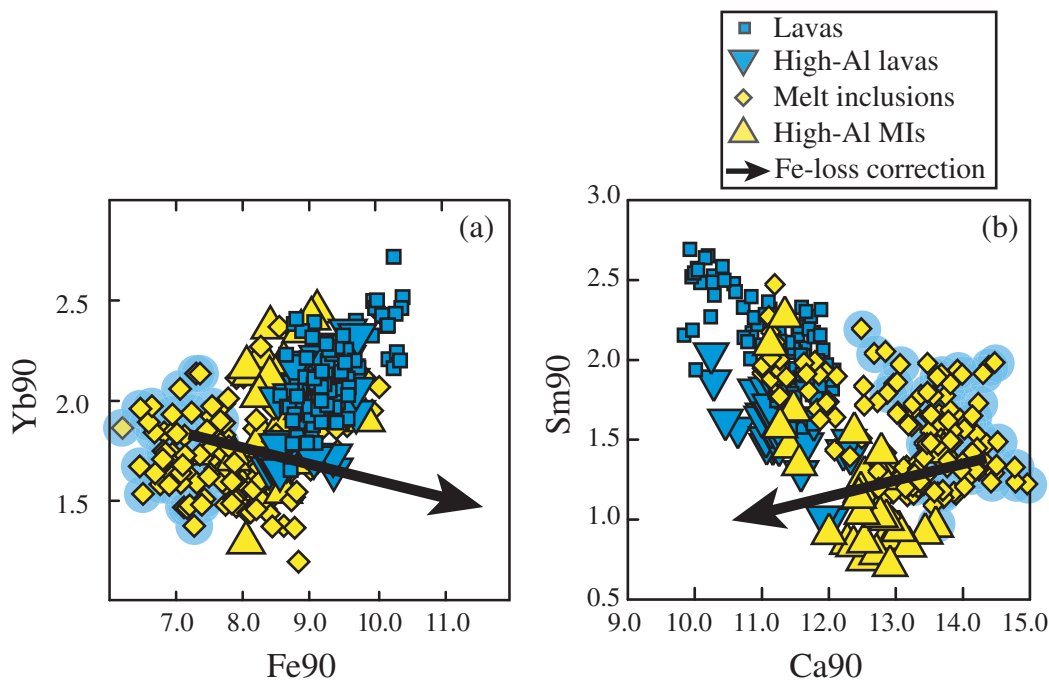


Fig. 3. Melt inclusion (after correcting for olivine overgrowth at the inclusion walls, referred to as ‘normal’ correction in the text) and lava compositions in equilibrium with Fe₉₀ olivine. (a) Yb₉₀ vs Fe₉₀. (b) Sm₉₀ vs Ca₉₀. The melt inclusions characterized by low FeO* contents (highlighted symbols) do not plot on the trends defined by the lavas and have therefore undergone Fe–Mg re-equilibration. We used the correlation in (a) to estimate the original FeO content in the melt inclusions that have been modified by re-equilibration (see text for details).

exhibit such large ranges, and such low concentrations in olivine, corrections for post-entrapment diffusion are minor. Furthermore, there are (imperfect) correlations in the lavas between Fe₉₀ and Y₉₀, Zr₉₀, and Yb₉₀, and between Ca₉₀ and Sm₉₀, for example (Fig. 3). The same samples that are offset from the trend of the lavas and have low FeO contents also have high CaO contents. Unlike the major element co-variations, the Fe-loss correction slopes for the major element/trace element plots are at a high angle relative to the trends in the lava data (Fig. 3). Post-entrapment re-equilibration thus seems to have occurred in the melt inclusions that display low FeO (and high CaO) contents and that deviate from the trend in the lavas.

These systematics suggest an approach to correction for post-entrapment re-equilibration. Instead of correcting all melt inclusions to a constant FeO value, we chose to use the Fe₉₀–Yb₉₀ correlation to estimate the initial FeO content in the melt inclusions (Fig. 3a). For the low-Fe melt inclusions that deviate from the main trend, we use their Yb₉₀ contents to estimate their true Fe₉₀ contents. Using these Fe₉₀ contents, we then correct the melt inclusion compositions for ‘Fe loss’ with Petrolog. For melt inclusions without measured trace element abundances, we could not use the Fe₉₀–Yb₉₀ correlation to estimate FeO contents. In this case, we estimated their ‘corrected’ FeO contents by comparison with the compositions of other ‘corrected’ melt inclusions from the same group within the same sample.

These melt inclusions were corrected to FeO = 8.9 wt % in the ARP73-10-03 sample, 8.7 in ARP74-11-18 and CH31-DR8, and 8.4 in G103-20-6. No correction for post-entrapment re-equilibration was required for ALV519-2-3, ALV521-1, ALV524-4 and ALV527-1, but the regular corrections for olivine overgrowth were performed. Only a few melt inclusions were corrected for Fe loss in samples ALV518-3-1, 2, 3 and 4 (only those with initial values below FeO* = 8.5 wt %), and ALV519-4-1. The final melt inclusion compositions, along with the type of correction performed, are reported in Electronic Appendix 2.

Although the method we develop to correct for the effects of post-entrapment re-equilibration processes has arbitrary aspects and is by no means perfect, we would argue that it is based on correlations observed in the lava data and is therefore likely to be more meaningful than assuming a single FeO content for all melt inclusions. Also, trace element variations are not strongly affected by these processes, and Fig. 2 shows that the melt inclusions record more chemical variability than the lavas, independent of correction scheme. As will be shown below, our conclusions are little influenced by the correction scheme adopted.

Major-element compositions

Corrected major element compositions for the inclusions are presented in Fig. 4a and b. Representative compositions are reported in Table 1. We divide the inclusions

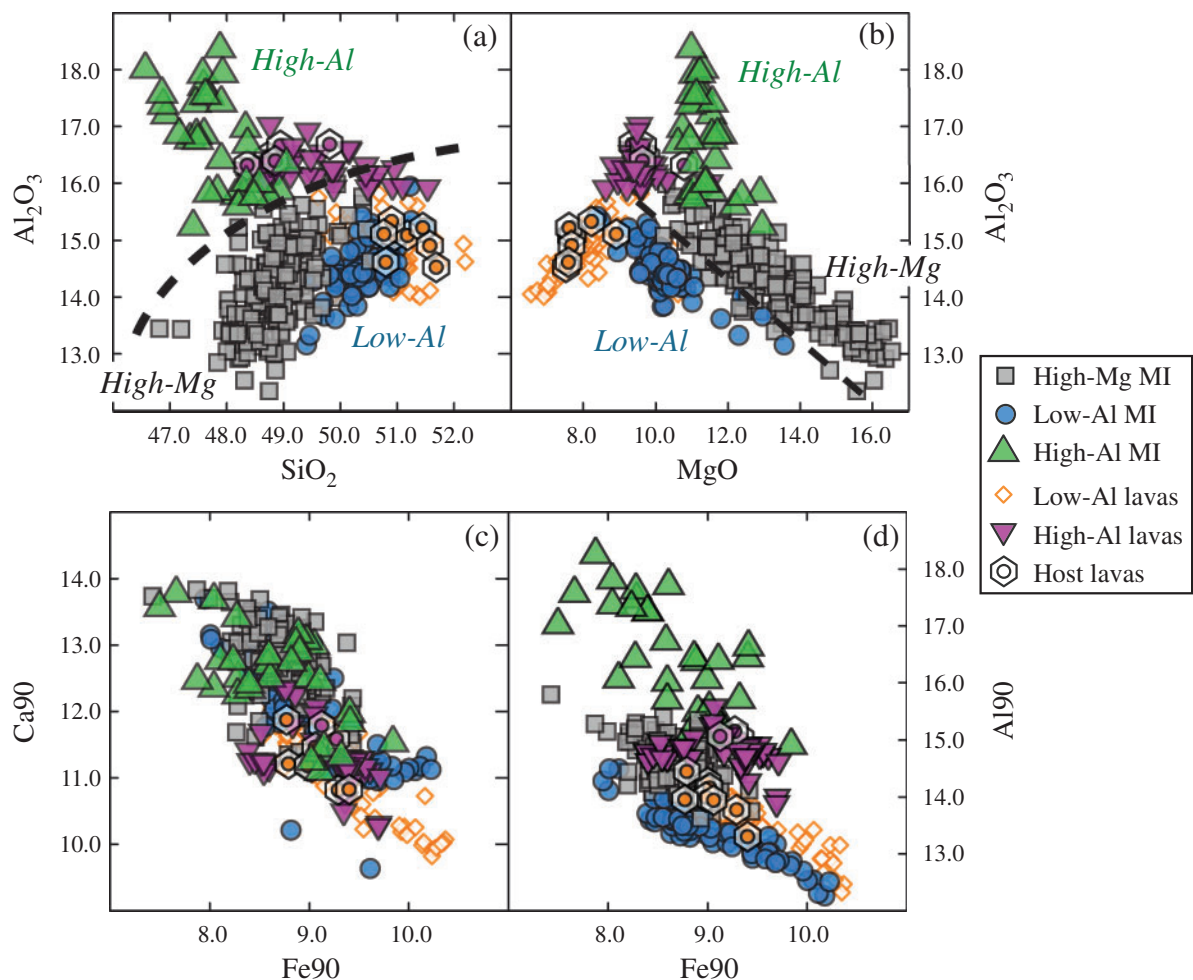


Fig. 4. Major element systematics (in wt %) in the FAMOUS melt inclusions after correction for olivine fractionation and possible Fe–Mg re-equilibration after entrapment (see text). (a, b) The compositional delimitations (dashed lines) and fields are reported for the different groups. The compositions of the host lavas and all the glasses (data from Gale *et al.*, in preparation) from the segment are also plotted. (c, d) To directly compare their parental melts, the melt inclusion and lava compositions were calculated to be in equilibrium with Fe_{90} olivine. The correlations in the lavas and melt inclusions are consistent, yet the melt inclusions display higher Ca_{90} concentrations on average, and a larger range in the Al_{90} contents.

into three groups based on their major element variations: (1) high-Mg melt inclusions trapped in Mg-number 88–92 olivines and characterized by the highest MgO contents (10.2–17.7 wt %) and intermediate Al contents; (2) low-Al melt inclusions hosted mostly in less primitive olivine phenocrysts (Mg-number 85.3–88.8) with lower average MgO (8.9–12.2 wt %), lower Al_2O_3 (13.4–16 wt %) and higher SiO_2 (49.4–51.5 wt %) contents; (3) high-Al melt inclusions trapped in Mg-number 88–90 olivines with high MgO contents (10.6–13 wt %), low SiO_2 (46.6–49.1 wt %) and high Al_2O_3 (15.3–18.4 wt %) concentrations. High-Al melt inclusions display the lowest concentrations in TiO_2 (as low as 0.40 wt %) and K_2O (as low as 0.003 wt %), but there are high-Mg inclusions that are almost as depleted.

Based on their major element compositions (Gale *et al.*, in preparation), the lavas can be divided into low-Al and

high-Al groups (Figs 4 and 5). Most FAMOUS glasses display compositions that are consistent with, although more differentiated than, the most enriched of the low-Al melt inclusions. A subset of ~30 lavas has distinctly higher Al_2O_3 , higher MgO and lower SiO_2 concentrations when compared with the rest of the basalts. The least extreme high-Al inclusions appear to be possible parents for these lavas (Figs 4 and 5). Most of the high-Al melt inclusions, however, extend to more extreme compositions far from those observed in any of the lavas. For example, maximum Al_2O_3 and minimum SiO_2 in the lavas are 17 wt % and 48.2 wt %, whereas the inclusions extend to >18 wt % Al_2O_3 and <47 wt % SiO_2 . Compositions corrected to Fe_{90} , which should overlap for common parental magmas, show limited overlap between high-Al lavas and inclusions (Fig. 3). Lavas that contain high-Al melt inclusions (ALV519-2-3, ALV519-4-1 and ALV527-1), all from

Table 1: Representative major (wt %) and trace element (ppm) compositions of the three groups of melt inclusions

| Sample: | ARP73-10-03-O110-MI1 | ARP73-10-03-O119-MI1 | ARP73-10-03-299* | CH31-DR8-OI2 | ALV519-4-1-OI4 | ALV518-3-1-OI3-MI1 | ALV518-3-3-OI3 | ARP74-11-18-OI8 | ALV519-2-3-OI1 | ALV519-2-3-OI7-MI2 | ALV519-4-1-OI7 | ALV527-1-OI1-MI1 |
|--------------------------------|----------------------|----------------------|------------------|--------------|----------------|--------------------|----------------|-----------------|----------------|--------------------|----------------|------------------|
| Group: | high-Mg | high-Mg | high-Mg | high-Mg | high-Mg | low-Al | low-Al | low-Al | high-Al | high-Al | high-Al | high-Al |
| SiO ₂ (wt %) | 48.578 | 49.034 | 48.915 | 48.604 | 49.589 | 50.257 | 50.651 | 50.828 | 47.601 | 47.583 | 47.61 | 46.888 |
| TiO ₂ | 0.528 | 0.577 | 0.603 | 0.501 | 0.664 | 0.933 | 0.876 | 0.593 | 0.4 | 0.42 | 0.405 | 0.446 |
| Al ₂ O ₃ | 13.157 | 13.067 | 13.43 | 14.342 | 15.296 | 13.876 | 15.041 | 14.211 | 17.744 | 17.959 | 16.889 | 17.407 |
| FeO* | 8.704 | 8.901 | 8.902 | 8.6 | 8.451 | 9.938 | 8.5 | 8.707 | 8.269 | 8.255 | 8.577 | 9.347 |
| MnO | 0.116 | 0.126 | 0.13 | 0.152 | 0.153 | 0.152 | 0.157 | 0.144 | 0.144 | 0.16 | 0.118 | 0.16 |
| MgO | 15.9 | 15.7 | 13.3 | 13.7 | 11.8 | 10.2 | 9.6 | 11 | 11.2 | 11.1 | 11.8 | 11 |
| CaO | 11.428 | 11.036 | 13.044 | 12.544 | 12.492 | 12.603 | 12.969 | 12.886 | 12.69 | 12.479 | 12.806 | 12.687 |
| Na ₂ O | 1.306 | 1.338 | 1.481 | 1.377 | 1.212 | 1.715 | 1.87 | 1.364 | 1.767 | 1.88 | 1.595 | 1.908 |
| K ₂ O | 0.013 | 0.015 | 0.063 | 0.008 | 0.131 | 0.123 | 0.13 | 0.046 | 0.008 | 0.009 | 0.011 | 0.007 |
| P ₂ O ₅ | 0.03 | 0.028 | 0.077 | 0.025 | 0.088 | 0.098 | 0.087 | 0.056 | 0.015 | 0.011 | 0.008 | 0.016 |
| Cr ₂ O ₃ | 0.095 | 0.086 | | 0.088 | 0.059 | 0.023 | 0.016 | 0.07 | 0.077 | 0.082 | 0.066 | 0.064 |
| S | 798 | 780 | 865 | 830 | 909 | 919 | 1056 | 858 | 836 | 914 | 882 | 917 |
| X _c | 0.19 | 0.19 | 0.17 | 0.12 | 0.08 | 0.12 | 0.06 | 0.17 | 0.06 | 0.05 | 0.15 | 0.10 |
| Mg-no. ol | 91.6 | 91.3 | 90 | 90.5 | 89.6 | 86.2 | 87.3 | 88.6 | 89.6 | 89.5 | 89.8 | 88.3 |
| Sc (ppm) | 33.9 | 32.1 | 35.3 | 35.3 | 38.3 | 48.7 | 38.7 | 35.8 | 38.7 | 40.7 | 40.2 | 43.9 |
| Ti | 3199 | 3384 | 3115 | 2940 | 3862 | 7135 | 4894 | 3501 | 2408 | 2421 | 2504 | 2610 |
| V | 194 | 178 | 169 | 188 | 117 | 292 | 222 | 226 | 160 | 155 | 160 | 174 |
| Cr | 724 | 645 | 554 | 590 | 451 | 290 | 156 | 355 | 459 | 462 | 449 | 377 |
| Mn (wt %) | 0.151 | 0.141 | 0.141 | 0.154 | 0.167 | 0.228 | 0.143 | 0.156 | 0.153 | 0.146 | 0.204 | 0.168 |
| Zn | 46.1 | 43.7 | 53.2 | 49.5 | 40.2 | | 57.4 | 57.4 | 37.7 | 42.2 | 40.7 | 46.8 |
| Ga | 9.5 | 9.3 | 8.3 | 9.6 | 8.8 | 15.8 | 10.8 | 10.1 | 9.8 | 9.4 | 8.9 | 10.4 |
| Rb | 0.385 | 0.309 | 2.011 | 0.093 | 3.548 | 4.659 | 3.086 | 0.756 | 0.101 | 0.086 | 0.139 | |
| Sr | 42.0 | 30.8 | 70.5 | 28.2 | 105.0 | 129.9 | 103.1 | 61.9 | 46.1 | 40.9 | 47.9 | 40.3 |
| Y | 14.9 | 15.1 | 13.4 | 13.9 | 15.1 | 25.4 | 18.8 | 15.3 | 16.2 | 17.6 | 16.9 | 18.5 |
| Zr | 20.5 | 18.9 | 31.0 | 16.9 | 39.8 | 65.6 | 47.3 | 26.7 | 16.6 | 18.1 | 17.3 | 18.5 |
| Nb | 0.524 | 0.627 | 4.43 | 0.347 | 7.503 | 9.066 | 6.404 | 2.364 | 0.461 | 0.304 | 0.465 | 0.219 |
| Ba | 2.48 | 4.06 | 26.19 | 1.29 | 44.34 | 54.09 | 38.44 | 13.15 | 1.38 | 0.53 | 1.33 | 0.31 |
| La | 0.83 | 0.728 | 2.709 | 0.539 | 4.287 | 5.418 | 4.032 | 1.755 | 0.546 | 0.533 | 0.582 | 0.539 |
| Ce | 2.56 | 2.17 | 5.89 | 1.27 | 9.51 | 12.59 | 9.41 | 4.65 | 1.48 | 1.23 | 1.56 | 1.48 |
| Pr | 0.501 | 0.451 | 0.906 | 0.325 | 1.279 | 1.766 | 1.363 | 0.733 | 0.311 | 0.3 | 0.362 | 0.313 |
| Nd | 2.746 | 2.775 | 4.002 | 2.281 | 5.71 | 8.774 | 6.558 | 4.018 | 1.941 | 1.908 | 2.093 | 2.025 |
| Sm | 1.101 | 1.187 | 1.315 | 1.081 | 1.414 | 2.779 | 1.875 | 1.052 | 0.777 | 0.883 | 0.81 | 0.984 |
| Eu | 0.476 | 0.508 | 0.5 | 0.437 | 0.59 | 1.004 | 0.74 | 0.558 | 0.413 | 0.443 | 0.404 | 0.477 |
| Gd | 1.74 | 1.894 | 1.87 | 1.736 | 1.935 | 3.753 | 2.712 | 2.364 | 1.419 | 1.655 | 1.758 | 1.752 |
| Tb | 0.333 | 0.349 | 0.326 | 0.311 | 0.339 | 0.671 | 0.478 | 0.352 | 0.309 | 0.362 | 0.386 | 0.348 |
| Dy | 2.284 | 2.501 | 2.068 | 2.327 | 2.389 | 4.185 | 3.217 | 2.423 | 2.533 | 2.718 | 2.396 | 2.731 |
| Ho | 0.5 | 0.521 | 0.527 | 0.482 | 0.515 | 0.892 | 0.658 | 0.599 | 0.588 | 0.636 | 0.697 | 0.62 |
| Er | 1.436 | 1.533 | 1.528 | 1.392 | 1.48 | 2.561 | 1.928 | 1.597 | 1.81 | 1.986 | 1.672 | 2.093 |
| Tm | 0.248 | 0.214 | 0.201 | 0.204 | 0.257 | 0.354 | 0.289 | 0.261 | 0.27 | 0.299 | 0.309 | 0.281 |
| Yb | 1.432 | 1.506 | 1.386 | 1.547 | 1.665 | 2.726 | 1.954 | 1.937 | 1.852 | 2.229 | 1.911 | 2.36 |
| Lu | 0.22 | 0.232 | 0.184 | 0.228 | 0.299 | 0.383 | 0.261 | 0.245 | 0.32 | 0.346 | 0.347 | 0.297 |
| Hf | 0.503 | 0.593 | 0.858 | 0.532 | 1.008 | 1.826 | 1.391 | 0.656 | 0.503 | 0.548 | 0.44 | 0.509 |
| Ta | 0.045 | 0.047 | 0.285 | 0.045 | 0.388 | 0.526 | 0.363 | 0.139 | 0.048 | 0.034 | 0.026 | 0.037 |
| Th | 0.024 | 0.037 | 0.342 | 0.016 | 0.46 | 0.569 | 0.428 | 0.192 | 0.008 | 0.009 | 0.016 | |
| U | 0.003 | 0.01 | 0.066 | 0.005 | 0.148 | 0.16 | 0.106 | 0.031 | 0.001 | 0.003 | 0.013 | |

All melt inclusions were corrected for post-entrapment modifications (see text for details of the correction procedure). The complete melt inclusion and host olivine dataset is reported in Electronic Appendix 2. X_c is the amount of post-entrapment correction that is used to calculate the concentrations of incompatible elements in the recalculated inclusion compositions.

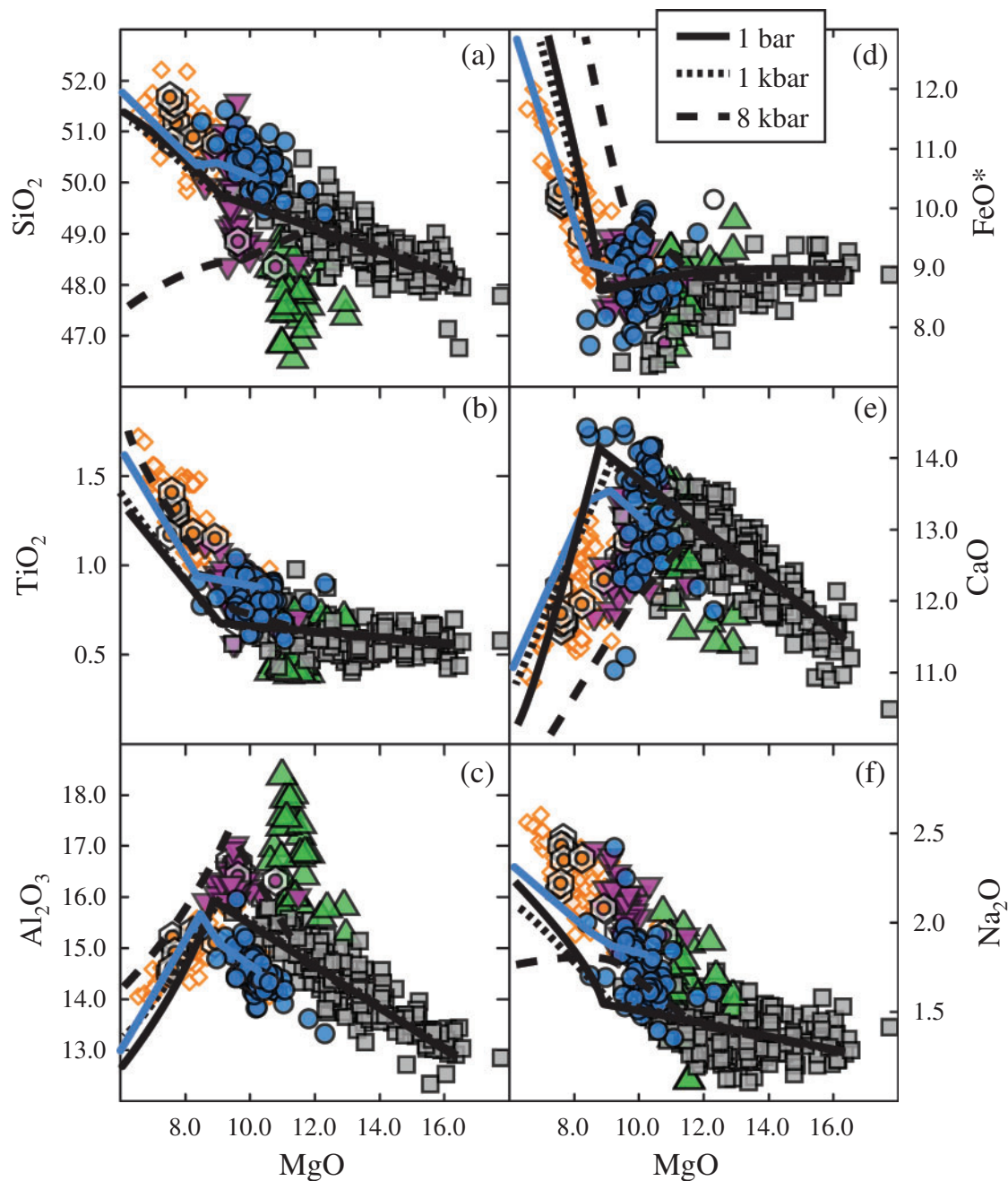


Fig. 5. Major element compositions (in wt %) of the FAMOUS melt inclusions after correction for post-entrapment modifications. The compositions of the host lavas and all the glasses from the segment (data from Gale *et al.*, in preparation) are also plotted. Liquid lines of descent were calculated using Petrolog at various pressures. FeO is reported as total iron (FeO*) expressed as Fe²⁺. Symbols as in Fig. 4.

Mt. Pluto, are high-Al basalts. It is noteworthy, however, that the high-Al basalts that contain olivines with high-Al melt inclusions also contain high-Mg inclusions (see Table 2 for details on which types of inclusions are found in which samples).

In general, the melt inclusions have a set of characteristics that distinguishes them from the lavas. They are

mostly higher in MgO, and hence more primitive, than any of the eruptive products. Many of them also are marked by high absolute CaO contents, as seen in Fig. 5e, and also in compositions corrected to Fo₉₀, apparent in the high Ca₉₀ concentrations seen in Fig. 4c. The inclusions are also low in incompatible elements. For example, the Na₂O contents of the high-Mg inclusions are often less

Table 2: Summary of compositions of host lava samples and their melt inclusions

| Sample name | Lava type | No. of high-Al MI* | No. of low-Al MI* | No. of high-Mg MI* | Host lava La/Sm | Av. La/Sm in MI | Range La/Sm in MI |
|-----------------|-----------|--------------------------|-------------------------|--------------------------|-----------------------|-----------------------|-------------------------|
| ALV0518-003-001 | low-Al | 0 | 11 | 7 | 2.01 | 1.68 | 0.8-2.37 |
| ALV0518-003-002 | low-Al | 0 | 3 | 2 | 2.01 | — | 1.79 ($n=1$) |
| ALV0518-003-003 | low-Al | 0 | 10 | 0 | 2.02 | 2.1 | 2.02-2.15 |
| ALV0518-003-004 | low-Al | 0 | 15 | 2 | 2.01 | 2.11 | 1.8-2.34 |
| ALV0519-002-003 | high-Al | 9 | 0 | 1 | 1.64 | 1.05 | 0.57-2.39 |
| ALV0519-004-001 | high-Al | 19 | 1 | 15 | 1.69 | 1.56 | 0.39-3.03 |
| ALV0521-001 | low-Al | 0 | 19 | 0 | 2.39 | 2.28 | 1.63-2.7 |
| ALV0524-004 | unknown | 0 | 15 | 0 | — | — | — |
| ALV0527-001 | high-Al | 4 | 0 | 6 | 1.45 | 1.41 | 0.51-2.88 |
| ARP1974-011-018 | low-Al | 0 | 1 | 12 | 2.07 | 2.05 | 1.55-2.72 |
| ARP1973-010-003 | high-Al | 0 | 0 | 130 | — | 1.59 | 0.45-2.63 |
| CH31-D8 | high-Al | 0 | 0 | 19 | 1.92 | 1.68 | 0.5-2.17 |
| GIL0103-020-006 | low-Al | 0 | 1 | 6 | 2.06 | 1.47 | 1.2-1.74 |
| NR DR 3-4 | low-Al | 0 | 0 | 8 | 3.26 | 1.98 | 1.12-3.02 |

*The number of melt inclusions from each melt inclusion group analyzed in each sample.

than 1.5 wt % Na₂O, and LLDs from these compositions do not intersect the lava compositions. The depletion is even more clearly apparent in the trace element compositions, as discussed below.

Trace-element compositions

A total of 117 melt inclusions were analyzed for their trace element compositions (Electronic Appendix 2), which makes this dataset unique in the sheer number of melt inclusions analyzed from a single ridge segment. We also include 23 analyses from Laubier *et al.* (2007) and 20 analyses from Shimizu (1998) for comparison. Representative compositions are reported in Table 1, and representative trace-element patterns for the different melt inclusion and lava groups are plotted in Fig. 6. The first striking aspect of the trace element data is its remarkable variability, particularly in extending concentrations to values far lower than found in any lava. The range of the most highly incompatible elements can be more than a factor of 100. Ba, for example, ranges from 0.3 to 59 ppm, and Th from 0.008 to 0.57 ppm. For comparison, minimum values of Ba and Th in the lavas are 15 ppm and 0.16 ppm, respectively. The most depleted compositions are typical of ultra-depleted melt inclusions, such as those reported by Sobolev & Shimizu (1993), Gurenko & Chaussidon (1995), Kamenetsky *et al.* (1998) and Danyushevsky *et al.* (2003, 2004). The (La/Sm)_N ratios of the inclusions (normalized to chondrite CI values;

McDonough & Sun, 1995) range from 0.25 (± 0.10 ; 2σ error) to 1.89 (± 0.25), in comparison with the range of 0.92–2.02 in the lavas (Gale *et al.*, in preparation). Highly incompatible trace element ratios in the melt inclusions also display large variability (Ba/Th = 47–164; Ba/Nb = 1.1–8.5; Nb/La = 0.41–2.21). The second aspect is that, in general, melt inclusion trace element concentrations are lower than in the lavas, even when the effects of fractionation are taken into account. This is evident in Fig. 7, showing that for both highly and moderately incompatible elements the concentrations in the inclusions are low. Figure 6 also shows that the most enriched inclusions graze the low end of the compositional field of the lavas, and the depleted inclusions are orders of magnitude lower in incompatible elements.

The three compositional groups identified in major elements also possess distinct trace element features. Both high-Mg and high-Al groups contain depleted melt inclusions (Fig. 6), but the compositions of the depleted inclusions differ between the groups. High-Al melt inclusions have high HREE concentrations for their low light REE (LREE) and MREE values. This characteristic is also observed in the high-Al lavas, which show an offset in HREE compared with the rest of the lava population (Figs 6 and 7; Gale *et al.*, in preparation). High-Mg melt inclusions do not have the steep slope in the HREE, and also extend to less depleted compositions. Their (La/Sm)_N ranges between 0.28 and 1.89 and Ba concentrations vary

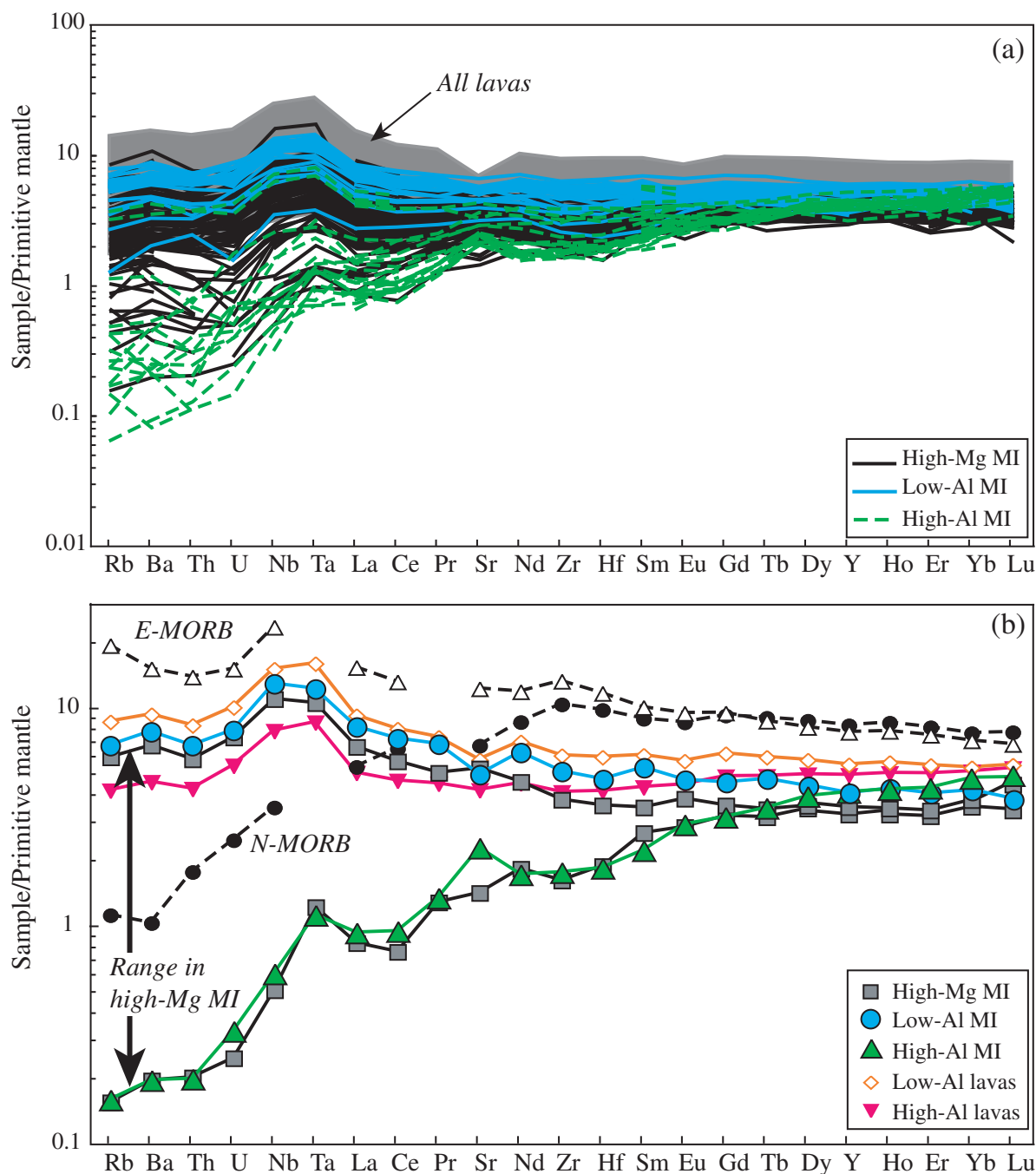


Fig. 6. (a) Primitive mantle (McDonough & Sun, 1995) normalized trace element compositions of melt inclusions and glass samples from the FAMOUS segment. All melt inclusion compositions have been recalculated to correct for post-entrapment processes (see text). (b) Representative primitive mantle (McDonough & Sun, 1995) normalized trace element patterns of the three groups of melt inclusions and two groups of lavas. Two melt inclusion end-members are shown for the high-Mg melt inclusions, a depleted and an enriched composition, to illustrate the large chemical variability in the high-Mg melt inclusions.

between 1.3 and 70 ppm. Low-Al melt inclusions have systematically higher concentrations for all the incompatible elements and display a smaller range of variations than the other melt inclusion groups. This enrichment is not

due solely to their slightly more evolved compositions, as will be shown in the discussion.

A major difference between the lavas and melt inclusions is the variation in highly incompatible trace element

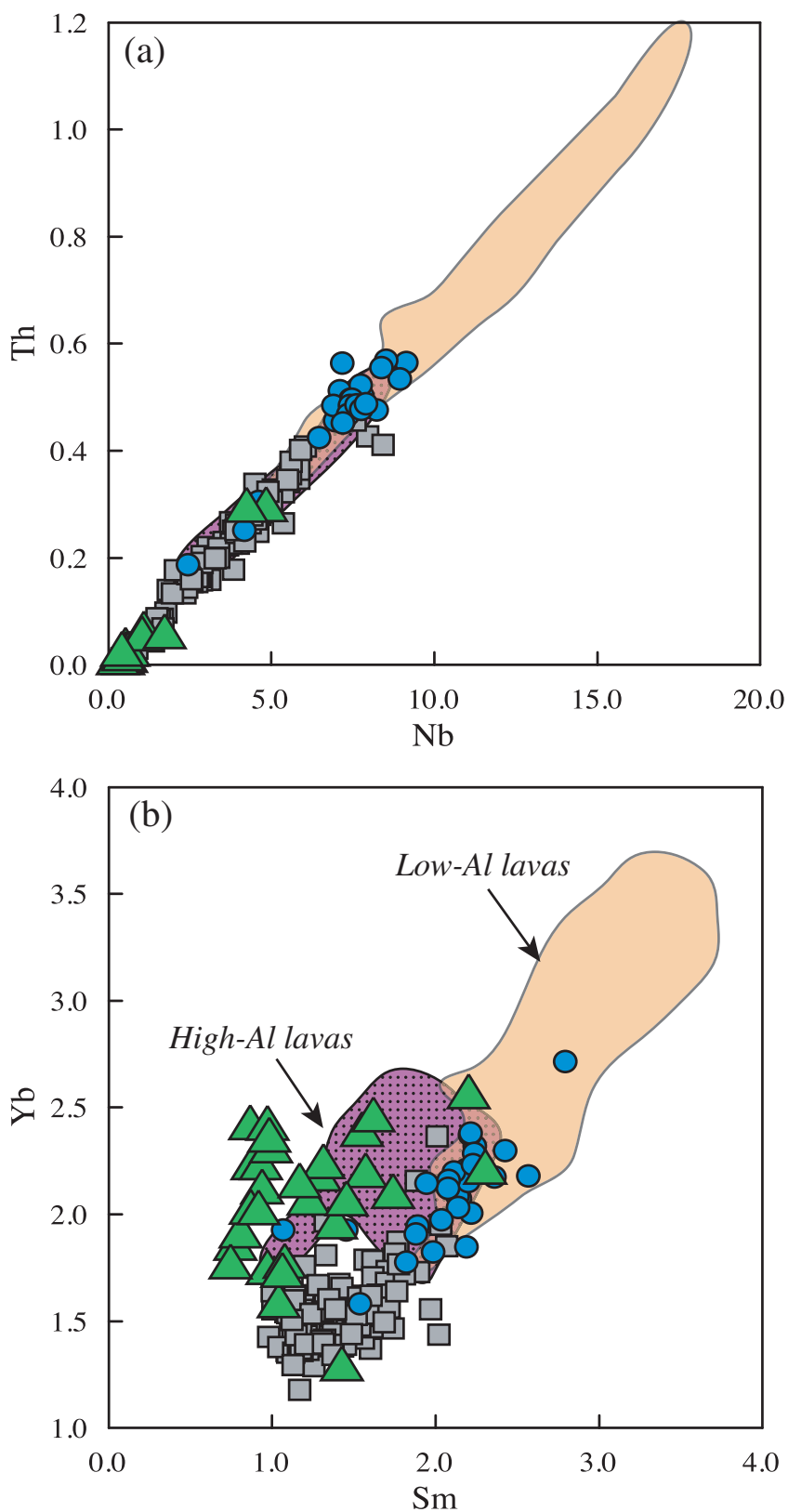


Fig. 7. Variation of Th vs Nb (a) and Yb vs Sm (b) (ppm) for the melt inclusions. Lava compositions from Gale *et al.* (in preparation) are indicated as compositional fields: low-Al lavas are represented as a filled area, high-Al lavas as a dotted area. Symbols as in previous figures.

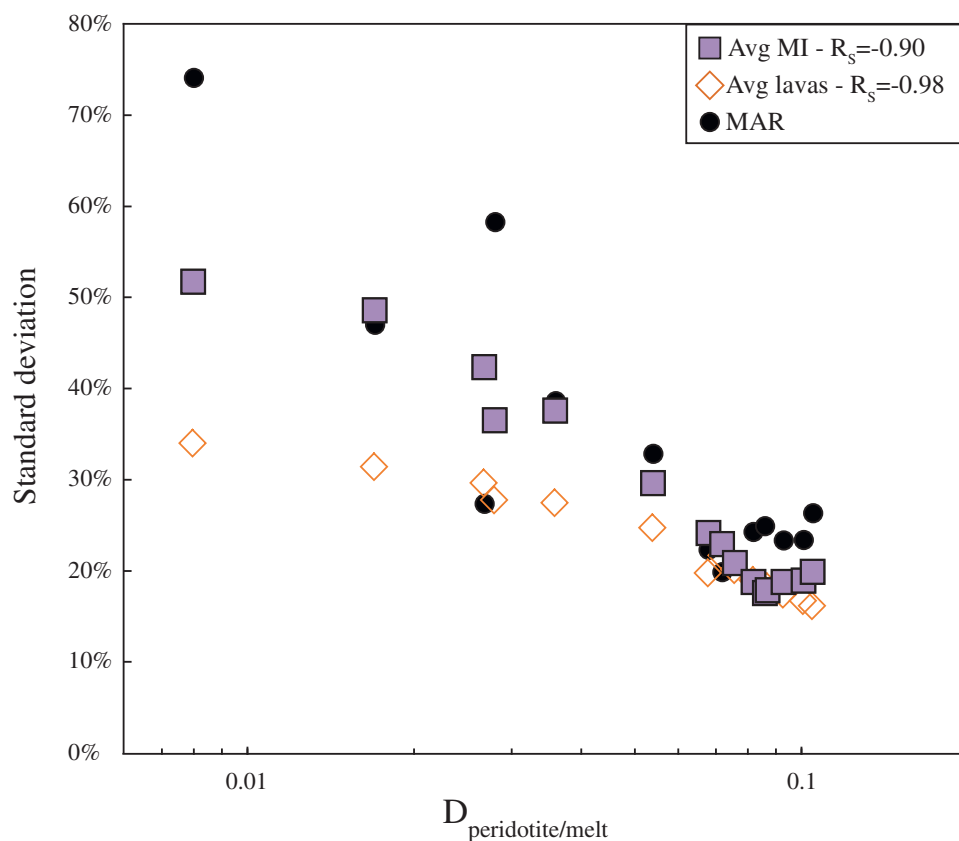


Fig. 8. Per cent standard deviation for elements measured in the olivine-hosted melt inclusions (laser ICP-MS data) and lavas from the FAMOUS segment as a function of $D_{\text{peridotite/melt}}$. Rank correlation coefficients are reported for each group. Variability in the Mid-Atlantic Ridge basalts from PetDB is shown for comparison (Cottrell *et al.*, 2002).

ratios. One of the intriguing characteristics of the FAMOUS lavas is that despite the substantial range in incompatible element abundances, the ranges in incompatible element ratios such as Ba/La (7–12) or Nb/La (1.5–1.8) is rather limited, even over a significant range in concentration. The less depleted inclusions bracket this range, but the most depleted inclusions show marked declines in highly incompatible element ratios, with Ba/La < 1 and Nb/La < 0.4.

DISCUSSION

Incompatible element diffusive re-equilibration

One of the outstanding questions from the work of Spandler *et al.* (2007) is whether trace elements such as the REE are influenced by diffusive re-equilibration, as are Fe and Mg. The systematics of the trace element variations can be used to test the importance of re-equilibration. Cottrell *et al.* (2002) demonstrated in a numerical model that variations in trace elements are strongly dependent on their diffusion coefficient. The data they evaluated indicated that REE abundances in plagioclase-hosted melt

inclusions are likely to be affected by re-equilibration, but the variability in natural olivine-hosted inclusions probably reflects the original chemical diversity at the time of entrapment. For the FAMOUS melt inclusions, the standard deviations for the trace element abundances in the different groups of olivine-hosted melt inclusions are inversely correlated with the values of mineral–melt partition coefficients during spinel peridotite melting (Fig. 8). Melt inclusions generally show more variability than the lavas for the highly incompatible elements, as would be expected if diffusive effects were minor. The correlation of the standard deviation (Spearman's rank correlation R_S) for the different elements with $D_{\text{peridotite/melt}}$ (Cottrell *et al.*, 2002) at a significance level of 0.999 is very good in the melt inclusions ($R_S = -0.90$; Fig. 8). For comparison, the FAMOUS lavas display a similarly good R_S value ($R_S = -0.98$). Also, our data show comparable correlations to the complete Mid-Atlantic Ridge (MAR) data (Cottrell *et al.*, 2002). The larger range in melt inclusion compositions compared with the lavas, and the similar systematics between inclusions and lavas, both argue against diffusive re-equilibration being an important process for the trace elements, because this process should modify

inclusion compositions to be inconsistent with what is observed in the lavas. These results are consistent with more recent measurements of diffusion of REE in Mg-rich olivine (Cherniak, 2010; Spandler & O'Neill, 2010) that are two to three orders of magnitude slower. Therefore, the trace element diversity in melt inclusions from this study is interpreted as being representative of the trapped compositions.

Origin of the diversity of melt inclusion compositions and their relation to the FAMOUS lavas

A conceptual paradigm for the interpretation of melt inclusions is that they reflect the diverse melts from a melting regime that arrive at the surface 'unpooled'. Lavas then result from mixing and fractionation of these melts to form a more average, pooled composition (e.g. Sobolev, 1996). In this case the melt inclusion compositions should be related to one another as diverse melts from a single melting column. Major and trace elements should be consistent within the inclusion population, with the most depleted inclusions from the top of the melting column corresponding to the highest degree melts at lowest pressures. These shallow, late-stage melts would have relatively high SiO₂, low incompatible element, low Al₂O₃ and high CaO contents (e.g. Sobolev & Shimizu, 1993; Sobolev, 1996). This scenario of diverse melts pooling to form the lavas was developed and supported on the basis of the global systematics of MOR basalt compositions (e.g. Klein & Langmuir, 1987; Langmuir *et al.*, 1992). A small set of melt inclusion data seemed to provide striking support, showing that within one sample, a whole range of compositions from low-degree, high-pressure melts to high-degree, low-pressure melts could all be present (Sobolev, 1996). As pointed out by Langmuir *et al.* (1992), however, the 'local vector' of the lavas at the surface is simply not consistent with variations within a single melting regime. Furthermore, the evidence from melt inclusions has never been tested by a comprehensive analysis of inclusions from multiple samples that can be compared with abundant lava compositions from the same region. The present study provides such an opportunity.

In general, the FAMOUS melt inclusions have more primitive and more variable compositions than the lavas, as apparent for the major elements in Fig. 5 and the trace elements in Figs 6 and 7. The range in SiO₂, CaO, Al₂O₃ and Na₂O is much greater for the inclusions than for the lavas. For example, at 12 wt % MgO, SiO₂ varies from 47 to 51 wt %, Al₂O₃ from 14 to 18 wt %, and Na₂O and TiO₂ vary by a factor of two. Because all of these variations occur within the domain where olivine alone is crystallizing, the inclusions must represent diverse parental melts. This could then imply that the melt inclusions are reflecting the diversity of melts from the melting column

that are mixed and homogenized to produce the lava compositions. The questions then are: first, are these melts related by different extents of melting within a melting column, and second, is a pooled melt inclusion composition the average parental melt for the FAMOUS lavas?

Major element variations for the melting column model should show coupled changes in Na₂O, TiO₂, Al₂O₃, SiO₂ and CaO. With greater extents of melting at shallower depths, Na₂O, TiO₂ and Al₂O₃ should decrease and correlate with one another as CaO increases (at least until the disappearance of clinopyroxene in the residue) and as SiO₂ increases as a result of the decreasing pressure. It is evident from inspection of Figs 3–6 that these predictions do not correspond to the data. The sequence of decreasing Al₂O₃ is high-Al, high-Mg and low-Al inclusions, but the high-Al inclusions have the most depleted trace element contents, the high-Mg melt inclusions a large range in trace elements and the low-Al inclusions the highest trace element contents. Furthermore, the depleted high-Al compositions also have the lowest SiO₂ contents.

Trace element variations are also not consistent with melting alone. For example, Fig. 7b shows that the high-Al inclusions are offset to lower Sm/Yb ratios compared with other inclusions and the low-Al lavas. The high-Al lavas share the low Sm/Yb ratios characteristic of the inclusions. The high-Al inclusions and lavas are also largely restricted geographically to the Mt. Pluto region in the rift valley. Melting column processes do not lead to variable Sm at the same Yb content. The high-Al group clearly requires a separate petrogenesis than the other compositions of the FAMOUS segment, a topic we return to below.

The low-Al inclusions are also problematic as representatives of the melting column. Their low Al₂O₃ contents would imply greater extents of melting, and yet they are more enriched in incompatible elements than the other two groups of inclusions. Many of these inclusions also have negative Sr and Eu anomalies, even though their Mg contents are all too high for plagioclase crystallization to have been significant.

The high-Mg melt inclusions as a group are the most promising melting column candidates. Their substantial range in depletion could result from a fractional melting process, and their very high MgO contents are consistent with mantle melts. We first turn to the origin of the high-Al and low-Al melt inclusions, and show that important aspects of their petrogenesis are related to crustal level processes. We then consider the high-Mg inclusions, whether they can be parental to the FAMOUS lavas, and what they reveal about mantle composition and processes in this region.

High-Al melt inclusions: evidence for melt–rock reaction in the lower crust

The high-Al melt inclusions extend to exceptionally high Al₂O₃ and low SiO₂, have very depleted trace element

compositions, and have distinctive low MREE/HREE ratios (e.g. Sm/Yb and Dy/Yb) compared with other inclusions. We suggest that these diverse characteristics are not caused by a single set of circumstances, but that the major element signature has become dominated by reaction processes in a cumulate mush pile in the crust, whereas the trace elements largely preserve the mantle history.

Our discussion of the origin of the high-Al melt inclusions needs to take place in the context of recent interest in the generation of high-Al basalts and melt inclusions that have been reported from various mid-ocean ridges. Two hypotheses have been suggested to explain the chemistry of the high-Al, low-Si basalts: (1) Lissenberg & Dick (2008) proposed, on the basis of their observations of gabbros from the Kane Megamullion (23°N, Mid-Atlantic Ridge), that high-Al basalts result from the reaction between primitive cumulates and migrating melt in the lower crust; (2) Eason & Sinton (2006) attributed the presence of high-Al basalts in the Galapagos Spreading Center to high-pressure fractionation of clinopyroxene. High-Al melt inclusions have also been reported (Kamenetsky *et al.*, 1998; Slater *et al.*, 2001; Danyushevsky *et al.*, 2003, 2004) and explained in terms of melt–rock reaction.

The FAMOUS segment provides a new perspective on these intriguing compositions because high-Al melts have been found both as melt inclusions and as lavas with similar major and trace element signatures. Therefore the petrological process generating high-Al melts is unlikely to be confined to small-scale portions of the crust or mantle, contrary to what has been proposed for some unusual melt inclusion compositions (Danyushevsky *et al.*, 2004). It must be a process that can generate volumes sufficient for volcanic eruptions.

The first question is whether reaction between primitive cumulates and migrating melts in the lower crust can generate these compositions. Lissenberg & Dick (2008) have proposed that the signal of high-pressure fractionation may be reproduced by melt–rock reaction at crustal levels, where migrating magma dissolves olivine and plagioclase and precipitates high-Mg clinopyroxene. Similarly, Drouin *et al.* (2009) argued that large clinopyroxene and plagioclase poikiloblasts within olivine-rich troctolites from Integrated Ocean Drilling Program (IODP) Hole U1309D (Atlantis Massif, Mid-Atlantic Ridge 30°N) result from intense melt–rock interaction. Although the occurrence of the high-Mg-number clinopyroxenes (Mg-number 86–91) is an important observation and an intriguing problem, we find the hypothesis of Lissenberg & Dick (2008) unlikely. They proposed a first step of troctolite assimilation by a high-Mg melt to produce high Al₂O₃ and MgO, and a decrease in SiO₂, FeO and CaO in the melt, leading to high MgO contents that would permit high-Mg-number clinopyroxene to

precipitate. However, consideration of phase diagrams illustrates that assimilation of olivine and plagioclase suppresses rather than enhances clinopyroxene stability. This is also evident in models of this process calculated using Petrolog, which show that the magma after assimilation is saturated with olivine only, followed in crystallization sequence by plagioclase, just as would be expected from assimilation of a troctolite. Therefore troctolite assimilation will not lead to poikilitic high-Mg-number clinopyroxene precipitation. In the absence of experimental data to the contrary, there is no evidence that reaction of a high-Mg liquid with olivine and plagioclase causes the precipitation of clinopyroxene, nor that this process mimics high-pressure crystallization leading to high-Al compositions.

The second question is whether true high-pressure crystallization of clinopyroxene, as advocated by Eason & Sinton (2006), can generate the high-Al signature. High-Mg-number clinopyroxenes in MORB have usually been interpreted as evidence for high-pressure fractionation, because of the expansion of the cpx stability field at the expense of olivine and plagioclase with increasing pressure (e.g. Grove *et al.*, 1992; Herzberg, 2004; Eason & Sinton, 2006; Villiger *et al.*, 2007). A general assessment of high-pressure crystallization as an explanation comes from calculations of LLDs for primitive melt inclusions from the FAMOUS segment using Petrolog, shown in Fig. 5. The calculations of LLDs are unable to reproduce the compositions of the high-Al melt inclusions from other inclusion compositions, even at extremely high pressures of crystallization (12 kbar) where clinopyroxene is usually the first to crystallize owing to its expanded phase stability. The high Al₂O₃ and low SiO₂ contents of high-Al melts cannot be obtained. Furthermore, CaO contents are relatively high (11.4–13.7 wt %) and Sc contents are on average higher in high-Al melt inclusions, ruling out a major role of early crystallization of clinopyroxene. This process alone, therefore, is insufficient to reproduce the extreme compositions of the high-Al melt inclusions.

Mantle–melt re-equilibration

Another model often called upon to produce MORB compositions is mantle–melt reaction at shallow levels (Kelemen *et al.*, 1995; Spiegelman & Kelemen, 2003; Spiegelman *et al.*, 2001; Collier & Kelemen, 2010). During their migration toward the surface, mantle melts produced at depth become undersaturated in pyroxene as they decompress adiabatically. Where undersaturated melts react with mantle peridotite, they dissolve pyroxene, producing a larger mass of melt, and precipitate a small amount of olivine. This is an incongruent reaction in which pyroxene dissolution produces both olivine and melt. Such reactions can lead to an increase in SiO₂, CaO and incompatible element concentrations in the melt whereas its Mg-number remains nearly constant, because the added orthopyroxene has higher concentrations of CaO, SiO₂,

and many incompatible elements than the removed olivine. Therefore, mantle–melt reaction can already be eliminated from the list of potential processes responsible for the generation of high-Al melts, as high-Al melts are characterized by low SiO₂ contents and highly depleted incompatible element concentrations, not the higher SiO₂ contents produced by orthopyroxene dissolution.

Melt–rock reaction in the lower crust

A successful model for the high-Al major element signature comes from assimilation of plagioclase-rich cumulates in the crust. Such a model is supported by the positive Sr anomaly that occurs in several of the compositions (Fig. 6; Sr/Sr* = 1.80–1.99). The occurrence of even higher positive Sr anomalies (Sr/Sr* = 2.1–34.6) has been reported in melt inclusions from several MORB samples from the MAR and East Pacific Rise (Kamenetsky *et al.*, 1998; Danyushevsky *et al.*, 2003, 2004) and in samples from Iceland (Slater *et al.*, 2001). These studies showed that these unusual inclusions are usually trapped in high-Fo olivine phenocrysts and display a range of incompatible element concentrations, but are most often ultra-depleted (Danyushevsky *et al.*, 2004). They display high Al₂O₃ and CaO contents and low Na₂O and TiO₂ contents. High-Al melt inclusions from our study also display an ultra-depleted signature in trace elements, and four of them exhibit a Sr anomaly; on average, high-Al melt inclusions are characterized by similar to slightly lower CaO contents and higher Na₂O than high-Mg and low-Al inclusions.

To explain the high-Sr melt inclusions found in MORB samples, Danyushevsky *et al.* (2004) proposed a model of dissolution–reprecipitation between a crustal gabbro (plagioclase + clinopyroxene + olivine) and an interstitial melt. These authors suggested that reactions between primitive melts and plagioclase result in the crystallization of aluminous spinel (Bedard *et al.*, 2000; Danyushevsky *et al.*, 2003, 2004). This possibility is strongly supported in the FAMOUS area. Fisk & Bence (1980) showed that FAMOUS sample ALV527-1-1, a high-Al lava that contains both high-Al and high-Mg melt inclusions, has three groups of spinel phenocrysts: (1) aluminous spinels [Cr-number = Cr³⁺/(Cr³⁺ + Al³⁺) = 0.22–0.32]; (2) Cr-rich spinels (Cr-number = 0.42–0.47) with reaction coronas; (3) spinels that are intermediate in Cr and Al and constitute the last generation of spinel to crystallize. Experiments were able to reproduce two of the spinels, but not the high-Al spinels (Fisk & Bence, 1980). The existence of the high-Al spinel and the experimental failure would be explained if aluminous spinel were the product of reaction between plagioclase and magma, as suggested by the researchers cited above.

On the strength of this evidence, we modeled assimilation of plagioclase + olivine and plagioclase + olivine + clinopyroxene cumulates by (1) a representative high-Mg melt inclusion and (2) a parental melt of the lavas (i.e.

in equilibrium with Fo₉₀ olivine) that is undersaturated with plagioclase and clinopyroxene at crustal pressures (Table 3). The compositions of the phases involved in the reaction match those at the onset of plagioclase and clinopyroxene crystallization along the LLDs of possible low-Al and high-Mg parent magmas. Two examples of the tested reactions are presented in Table 3. All reactions produce an increase in Al₂O₃ and a decrease in SiO₂ and FeO, along with positive Sr anomalies and a depletion in incompatible elements (Fig. 9). These are robust characteristics of the calculations independent of parental magma. We therefore attribute the major element features and the positive Sr anomalies of the high-Al melt inclusions to crustal assimilation processes.

Most of the trace element characteristics of the high-Al inclusions, however, cannot be replicated by this assimilative process. In particular, diluting the incompatible elements enough is not possible without creating a high Ba/Th ratio, and the low MREE/HREE ratios are never recovered (Fig. 9). This remains true even with the addition of clinopyroxene in the cumulate. These simple calculations show that the very depleted highly incompatible element contents and the low MREE/HREE ratios in most of the high-Al inclusions cannot be the result of assimilation and/or fractional crystallization processes. A similar conclusion was reached by MacLennan (2008a) for Icelandic inclusions and by Gurenko & Sobolev (2006) for Icelandic glasses. We view these characteristics of the high-Al inclusions, therefore, as indicative of their parental magmas. Models for their occurrence are presented in a subsequent section.

There is one other important and serendipitous result of these calculations. One of the curiosities of MORB has been the existence of very high-An feldspars (up to An₉₀), which occur in FAMOUS lavas (Stakes *et al.*, 1984; le Roex *et al.*, 1996) and are rather widespread in plagioclase-phyric basalts (e.g. Nielsen *et al.*, 1995; Sours-Page *et al.*, 1999). In general, primitive MORB are in equilibrium with An₈₅ plagioclase, although of course this varies with Na₂O content. No observed lavas at the surface have An₉₀ plagioclase on the liquidus, so the relatively common occurrence of such phenocrysts and megacrysts has been mysterious. They are often large with complex zoning profiles and a ‘moth-eaten’ texture, suggesting a history of disequilibrium. Troctolite assimilation and recrystallization provide a simple solution to this mystery. In the assimilation models, there is early appearance of An₉₅ plagioclase around MgO = 11 wt % at 1 kbar. Indeed, Nielsen *et al.* (1995) experimentally generated high-An plagioclase phenocrysts by adding olivine and plagioclase to their starting compositions. Troctolite assimilation in the lower crust could then be a mechanism to generate the high An contents, the very large plagioclase phenocrysts with complex resorption patterns and

Table 3: Compositions and proportions used in our model of melt–cumulate reactions

| | (1) High-Mg melt | (1) Calc. melt | (2) Parental melt | (2) Calc. melt | High-Al melt |
|--------------------------------|------------------------|----------------------|-------------------------|----------------------|-----------------|
| SiO ₂ (wt %) | 48.90 | 46.70 | 49.19 | 47.34 | 46.58 |
| TiO ₂ | 0.554 | 0.355 | 0.86 | 0.56 | 0.618 |
| Al ₂ O ₃ | 14.11 | 18.59 | 12.79 | 18.52 | 18.05 |
| FeO* | 8.32 | 6.66 | 9.60 | 6.80 | 8.59 |
| MgO | 14.06 | 12.89 | 14.51 | 11.08 | 11.3 |
| CaO | 13.00 | 12.78 | 10.93 | 12.73 | 12.74 |
| Na ₂ O | 1.428 | 1.406 | 1.79 | 1.66 | 1.768 |
| K ₂ O | 0.019 | 0.017 | 0.10 | 0.07 | 0.009 |
| Cr ₂ O ₃ | 0.091 | 0.873 | 0.20 | 1.16 | 0.064 |
| Sr (ppm) | 42.31 | 67.25 | 100.0 | 104.8 | 45.57 |
| Y | 15.14 | 9.39 | 18.48 | 11.85 | 17.68 |
| Zr | 20.85 | 12.84 | 40.79 | 25.23 | 18.57 |
| Nb | 0.631 | 0.388 | 5.12 | 3.13 | 0.415 |
| Ba | 3.479 | 3.832 | 29.49 | 19.83 | 1.300 |
| La | 0.765 | 0.520 | 3.21 | 2.03 | 0.607 |
| Ce | 2.338 | 1.533 | 7.64 | 4.82 | 1.591 |
| Pr | 0.488 | 0.313 | 1.11 | 0.71 | 0.343 |
| Nd | 2.983 | 1.892 | 5.49 | 3.49 | 2.163 |
| Sm | 1.205 | 0.752 | 1.71 | 1.09 | 0.905 |
| Eu | 0.491 | 0.351 | 0.64 | 0.46 | 0.450 |
| Gd | 1.875 | 1.167 | 2.49 | 1.60 | 1.722 |
| Tb | 0.350 | 0.215 | 0.45 | 0.28 | 0.345 |
| Dy | 2.483 | 1.540 | 3.02 | 1.94 | 2.658 |
| Ho | 0.530 | 0.328 | 0.66 | 0.42 | 0.632 |
| Er | 1.524 | 0.943 | 1.89 | 1.21 | 1.883 |
| Yb | 1.583 | 0.974 | 1.87 | 1.18 | 2.106 |
| Lu | 0.254 | 0.159 | 0.29 | 0.19 | 0.332 |
| Hf | 0.583 | 0.359 | 1.14 | 0.70 | 0.524 |
| Ta | 0.052 | 0.032 | 0.30 | 0.19 | 0.042 |
| Th | 0.031 | 0.019 | 0.32 | 0.19 | 0.016 |
| U | 0.0087 | 0.0053 | 0.11 | 0.07 | 0.0067 |
| Sr/Sr* | 1.17 | 2.88 | 1.15 | 1.90 | 1.79 |
| Eu/Eu* | 1.00 | 1.14 | 0.95 | 1.05 | 1.100 |
| X _{melt} | | −0.6 | | −0.6 | |
| X _{plag} | | −0.275 | | −0.29 | |
| X _{cpx} | | 0 | | −0.05 | |
| X _{Cr spl} | | −0.04 | | −0.04 | |
| X _{ol} | | −0.085 | | −0.02 | |
| X _{Al spl} | | 0.02 | | 0.02 | |
| X _{Cr spl} | | 0.005 | | 0 | |
| X _{melt calc} | | 0.975 | | 0.98 | |

The mineral compositions represent average compositions of Mg-number 86 olivine and An₈₃ plagioclase phenocrysts from FAMOUS samples, and spinel compositions from ALV519-4-1 (Fisk & Bence, 1980). Two scenarios with their starting and final melt compositions (a high-Mg trace element depleted melt inclusion and an average parental melt of the low-Al lavas) and the reaction coefficients are reported. Only the results of the assimilation from the high-Mg melt inclusion are shown in Fig. 9. The composition of a high-Al melt inclusion is reported for comparison. $Sr/Sr^* = [Sr_N/\sqrt{(Ce_NNd_N)}]$; $Eu/Eu^* = [Eu_N/\sqrt{(Sm_NGd_N)}]$, where the concentrations are normalized to the composition of CI chondrite (McDonough & Sun, 1995).

zoning profiles, the highly phyrlic lavas and the very low TiO₂ contents of the high-An hosted melt inclusions (e.g. Sours-Page *et al.*, 1999).

The calculations also show further the problems with the Lissenberg & Dick (2008) suggestion that troctolite assimilation leads to high-Mg clinopyroxene. After troctolite assimilation, clinopyroxene crystallizes in the hybrid melt at similar or slightly lower temperature and MgO contents in the melt (7.9 wt %) compared with those prior to assimilation. The first cpx to crystallize has a Mg-number of 85 and is in equilibrium with an An₇₈ plagioclase and Mg-number 84 olivine. Clinopyroxenes that crystallize from the melt after assimilation are not characterized by higher Mg-number than those expected from a normal melt. We return to the origin of the poikilitic high-Mg-number clinopyroxenes further below.

Low-Al melt inclusions: evidence for crustal mixing between high-Mg inclusions and crustal lava compositions

The low-Al melt inclusions occur in lower Fo olivines and appear to be closer in composition to the low-Al lavas of the FAMOUS segment. Careful consideration of their major and trace element characteristics, however, suggests they are in fact hybrid compositions formed by mixing between high-Mg inclusion and low-Al lava compositions.

The first puzzle regarding the low-Al melt inclusions is their low Al₂O₃ content. Lower Al₂O₃ can be produced by higher extents of melting of the mantle, but these inclusions have higher incompatible element and HREE abundances than the high-Mg inclusions (Figs 6 and 7). Inspection of Fig. 7 also shows that low-Al inclusions have negative Sr anomalies, suggesting removal of plagioclase; however, their steep negative slope on the MgO–Al₂O₃ diagram and their high MgO contents show that plagioclase would not have crystallized. The inclusions also have very steep slopes on MgO–Na₂O and MgO–TiO₂ diagrams, which are inconsistent with the LLDs calculated from the inclusion compositions (Fig. 5). These slopes are even steeper than what would be observed for ol + plag + cpx crystallization at far lower MgO contents.

All of these observations are rectified if the low-Al inclusions are mixtures between high-Mg inclusion and low-Al lava compositions. For example, Fig. 10 shows a plot of Sr vs Pr content for the high-Mg and low-Al inclusions. Data for the high-Mg melt inclusions form a trend that intersects the origin, consistent with the similar geochemical behavior of these two elements in the absence of plagioclase. The low-Al melt inclusions form a scattered array ranging from the field of high-Mg inclusions towards the lavas, suggesting mixing. The mixing hypothesis also explains how these low-Al melt inclusions could have negative Sr anomalies at such high MgO contents, as the low-Al lavas will impart their negative Sr anomaly signature to the

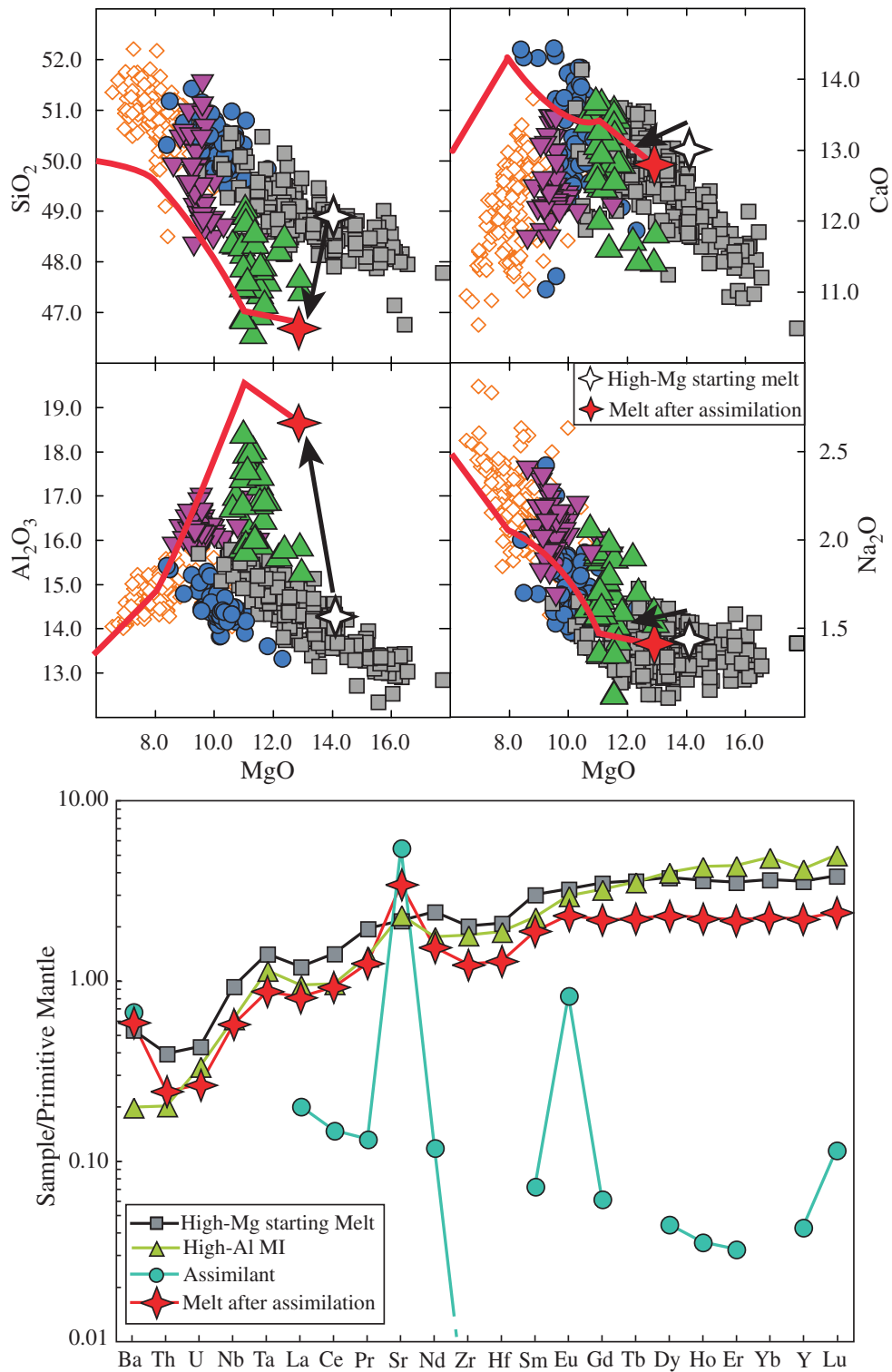


Fig. 9. Major and trace element modeling of the assimilation of a plagioclase-bearing cumulate by a high-Mg trace-element depleted melt inclusion, and the later crystallization path of the resultant melt at a pressure of 1 bar. The starting and final melt compositions and the melt and mineral proportions are given in Table 3. Arrows represent the chemical changes produced by the assimilation process. The trace element composition of the assimilant (Table 3) is shown in the trace element diagram. Although the assimilation process can account for the major element characteristics of the high-Al melt inclusions, the low MREE/HREE ratios are not reproduced. Symbols as in previous figures.

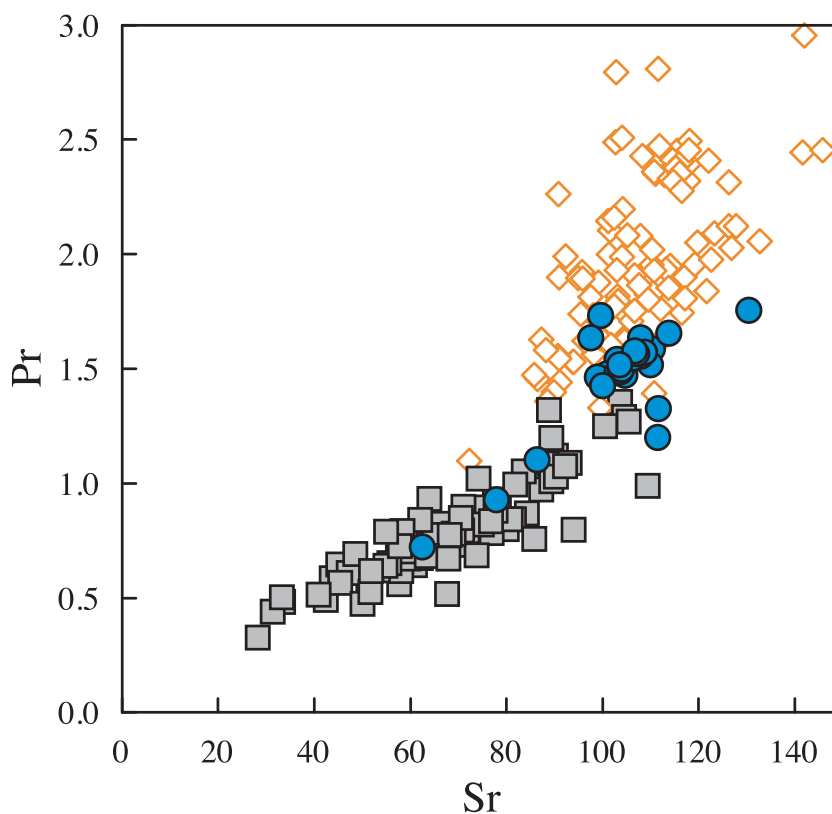


Fig. 10. Variation of Pr vs Sr (ppm) in the high-Mg and low-Al melt inclusions and low-Al lavas. This ratio is changed only by plagioclase fractionation; the low-Al melt inclusions are too high in MgO to have plagioclase on the liquidus. The low-Al melt inclusion compositions are best explained by mixing between the high-Mg melt inclusions and differentiated low-Al lavas. Symbols as in previous figures.

low-Al inclusions. Similarly, their steep slope on the MgO–TiO₂ and MgO–Na₂O plots (Fig. 5), and their lower Al₂O₃ contents are also explained if the melt inclusions result from this mixing process. Also, it would be for this reason that the trace element patterns of the low-Al inclusions, seen in Fig. 6, so closely match the lavas but at lower overall abundances. Injection of a high-Mg melt composition into a body of magma with a low-Al lava type composition would lead to crystallization of moderately high Fo olivine, and incorporation of these hybrid low-Al type compositions into the olivines.

Origin of the high-Mg melt inclusions

It thus appears that two of the three melt inclusion groups are strongly influenced by mixing and hybridization processes taking place within the crust or shallowest mantle lithosphere. The third type of inclusion, the high-Mg inclusions, provide an initial melt composition that is then modified by crustal processes to produce the high-Al major element signature, and the low-Al major and trace element signature. The ‘mantle signal’, then, lies in the overall diversity of the high-Mg inclusions (as well as the diagnostic trace element characteristics of the high-Al inclusions).

The high-Mg melt inclusions are characterized by a large range of trace element compositions, from ultra-depleted to transitional MORB. At the outset, fractional crystallization can be easily ruled out as a major factor in controlling the trace element variations, as major elements show that the inclusions crystallized only olivine before their entrapment in the host crystals (Fig. 5), and incompatible element ratios are unchanged by olivine crystallization (Fig. 11). The large trace element variations in the high-Mg and high-Al melt inclusions must therefore be interpreted in terms of mantle melting processes, with a potential role for mantle source heterogeneity.

Certain aspects of the trace element data might appear to be consistent with a simple melting sequence (Figs 6 and 7). For example, the linear trend in the La/Sm vs La plot in Fig. 12a is consistent with batch melting. However, extreme variability in incompatible trace element ratios such as Ba/La (2.4–14.9) and Nb/La (0.63–1.87) cannot be accounted for by batch melting. The curvature of the high-Mg melt inclusion trend in the Ba/La vs Ba plot (Fig. 12b) appears instead to support a fractional melting process, which would be consistent with the concept of the melt inclusions representing fractional melts from the melting regime (e.g. Sobolev & Shimizu, 1993; Gurenko &

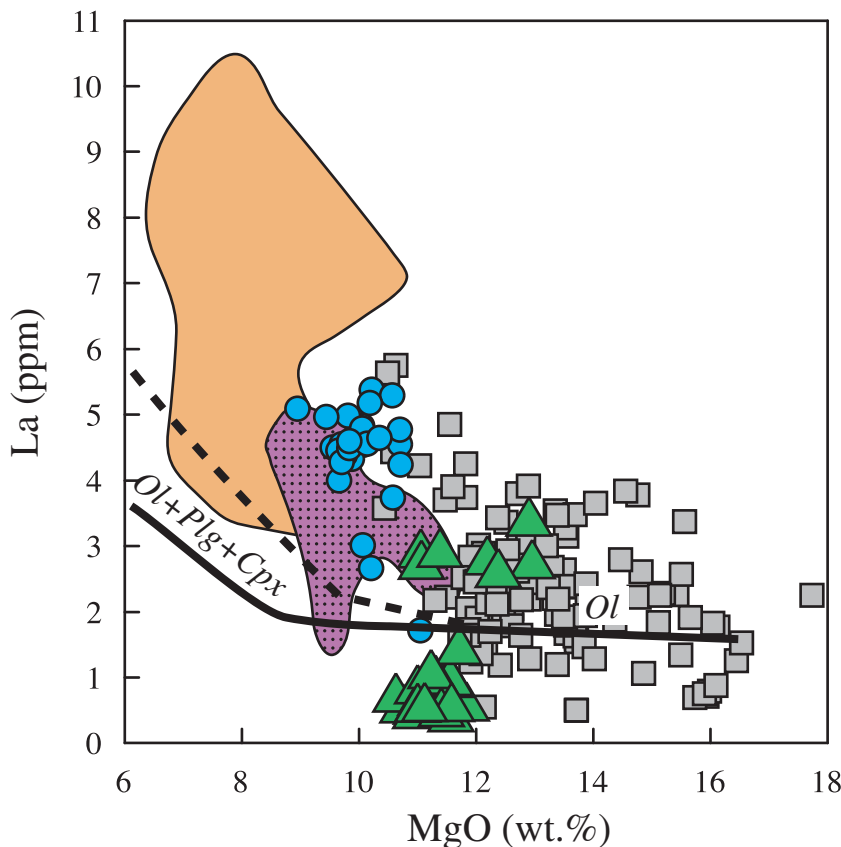


Fig. 11. Variation of La vs MgO in melt inclusions. Fractional crystallization trends from a high-Mg melt inclusion at 1 bar (continuous line) and 8 kbar (dashed line) are shown. Fractionation of olivine only cannot account for the large variability in La. Symbols as in previous figures. Compositional fields are indicated for the FAMOUS glass samples (Gale *et al.*, in preparation).

Chaussidon, 1995; Sobolev, 1996). Closer inspection of the data, however, reveals that fractional melting is also not a sufficient model to account for the data.

Because many of the fractional melts produced in the melting regime are ultimately pooled, evaluation of fractional melting is difficult. The data need to be considered as potential mixtures of diverse fractional melts. To address the question of whether the trace element variations in the melt inclusions could be generated by mixing between instantaneous near-fractional melts, we have modeled behavior of trace elements during polybaric melting using the algorithm pHMELTS (program `adiabat.lph`; Smith & Asimow, 2005). pHMELTS provides a useful template for trace element modeling by varying residual mineralogy and partition coefficients during melting (Figs 12–14). In all the melting models presented below, we used an oxygen fugacity of QFM and the set of partition coefficients provided by default in the program that vary with pressure. As will be shown below, important constraints come from the systematics of the melt inclusion compositions, which do not depend on the choice of partition coefficient values.

We also need to select a source composition that allows us to match the most enriched values in the highly incompatible trace element ratios (e.g. Ba/La as high as 14.9; Nb/La as high as 1.87). The composition of a depleted MORB mantle (DMM; Salters & Stracke, 2004) is far too depleted to produce the transitional (T)-MORB compositions of the most enriched high-Mg melt inclusions. A more reasonably enriched source composition, reported in Table 4, is composed of 60% DMM (Salters & Stracke, 2004) and 40% of the incompatible element-enriched source (‘metasomatized source’ in Table 4) that was previously defined to explain the enriched lava compositions at the Lucky Strike and Menez Gwen segments north of FAMOUS (Gale *et al.*, 2011).

Given a source that can account for the most enriched compositions in the high-Mg melt inclusions, we also need to reproduce the most depleted compositions of the high-Mg group (with Ba/La ratios as low as 2.4), as well as the strong curvature in the high-Mg melt inclusion data in the Ba/La vs Ba plot (Fig. 12b). Both features require a near-fractional melting process, with a maximum amount of 2 wt % melt retained in the residue. Higher

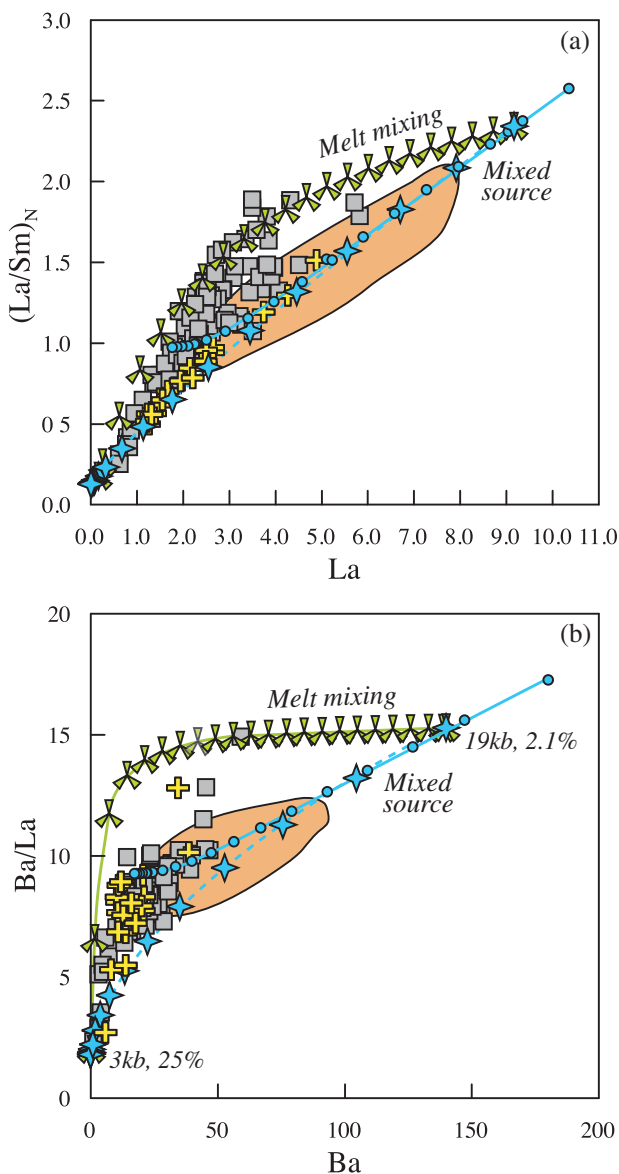


Fig. 12. $(La/Sm)_N$ vs La (a) and Ba/La vs Ba (b) in high-Mg melt inclusions. Decompression melting curves from a mixed source (Table 4) are shown for near-fractional instantaneous (stars; 2% of melt is retained in the residue) and pooled (circles) melts. Pressures (in kbar) and melting extents (F in wt %) are indicated; symbols on the melting curves represent 1 kbar decompression steps. A mixing curve between a low-degree and a high-degree instantaneous near-fractional melt is also shown. Crosses track the compositions of melt inclusions that plot along the melting curve in the $(La/Sm)_N$ vs La plot (a). It should be noted that these compositions show highly variable Ba/La ratios and are not consistent with a melting trajectory in the Ba/La vs Ba plot (b). Symbols as in previous figures. Lava compositions in equilibrium with F_{90} are reported as compositional fields (Gale *et al.*, in preparation).

melt porosity in the source would not only be physically unrealistic but would also preclude the extremely low Ba/La values in the most depleted compositions.

Because fractional melting leads to such large changes in incompatible element ratios, and because each increment of melting yields a potential mixing end-member, it would appear that mixtures of fractional melts might account for any of the data, and this is a hypothesis that would be difficult to refute. For example, in Fig. 12b, the high-Mg inclusions occupy the field enclosed by pure fractional melting and a mixing curve between a deep low-degree fractional melt and a shallow high-degree fractional melt. When combined with the potential effects of mantle heterogeneity, it becomes difficult to refute any model.

In fact, the situation is not so dire, and it can be simply shown that mixing of diverse fractional melts from a single source does not account for the data. Mixing models require that the sequence of compositions have the same relative placement between mixing end-members in all aspects of compositional space. Figure 13 highlights one group of high-Mg melt inclusions with a different symbol to make use of this simple test. In Fig. 13a, the open cross symbols plot exactly on the mixing line between smallest and greatest degree fractional melts. The remaining inclusion data plot closer to the curve of unmixed fractional melts. In Fig. 13b the positions are reversed: the open cross symbols are furthest from the mixing curve, and the remaining data plot along it. Therefore no mixing model of fractional melts can account for these data.

In contrast, source heterogeneity does account for the spectrum of compositions. Figure 13 also illustrates melting curves for diverse sources. In contrast to the case for fractional melting of a single source, the two groups of high-Mg melt inclusions show the same relative positions with respect to source variation. The open crosses plot between the curves for pooled fractional melts of the intermediate source and fractional melts of the enriched source, whereas the remaining data plot along the extension of the pooled melt curve for the intermediate source. This systematic variation suggests further exploration of source heterogeneity as an explanation for the diversity of the high-Mg inclusions.

Source heterogeneity is also strongly supported by a parallel study of the lavas from the FAMOUS ridge segment carried out by Gale *et al.* (in preparation). Lavas from this region display substantial variations in their radiogenic isotope composition that correlate with their trace element ratios. For example, La/Sm, La/Yb, Zr/Nb and Nb/La in the lavas correlate with Pb and Nd isotope compositions. Gale *et al.* (in preparation) have developed a straightforward model that accounts well for both trace element and isotope diversity in the erupted 'normal' lavas (a separate petrogenesis is required for the high-Al lavas, as for the high-Al melt inclusions, as discussed below). The model simply creates an array of sources that are mixtures between two end-members—a metasomatized enriched source created by addition of a low-degree melt of the

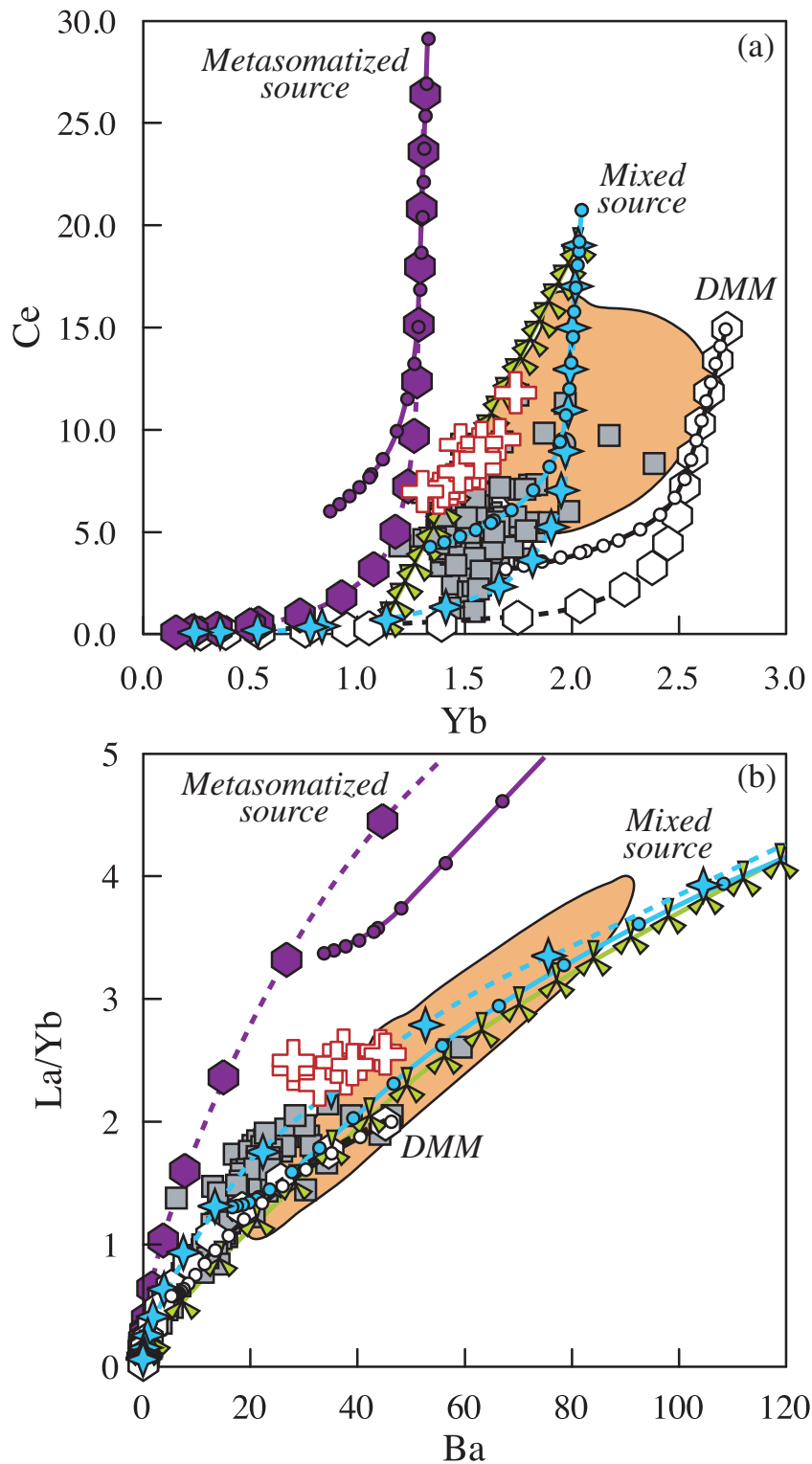


Fig. 13. Ce vs Yb (a) and La/Yb vs Ba (b) in high-Mg melt inclusions. Decompression melting curves from a mixed source (Fig. 12; between 19 kbar, 2.1% and 3 kbar, 25%), DMM (Salters & Stracke, 2004; 21 kbar, 2.6% to 3 kbar, 25%) and a metasomatized source (19 kbar, 2.8% to 3 kbar, 25.5%) are shown for near-fractional instantaneous melting (2% melt retained in the residue). Symbols on the melting curves represent 1 kbar decompression steps. Pooled melts (circles) are also plotted for the three source compositions. The mixing curve between a low-degree and a high-degree instantaneous near-fractional melt from the mixed source (Fig. 12) is also shown. Compositional fields (in equilibrium with $F_{0.90}$) are indicated for the FAMOUS low-Al lavas (Gale *et al.*, in preparation). Open crosses represent melt inclusions that plot in the vicinity of both the mixing trajectory and the melting curve of the metasomatized source in the Ce vs Yb diagram (a). In the La/Yb vs Ba plot (b), these melts have a constant La/Yb ratio and plot towards the melting curve of the metasomatized source rather than close to the mixing curve. This observation shows the contribution of source heterogeneity to the generation of the compositional variability observed in the high-Mg melt inclusions.

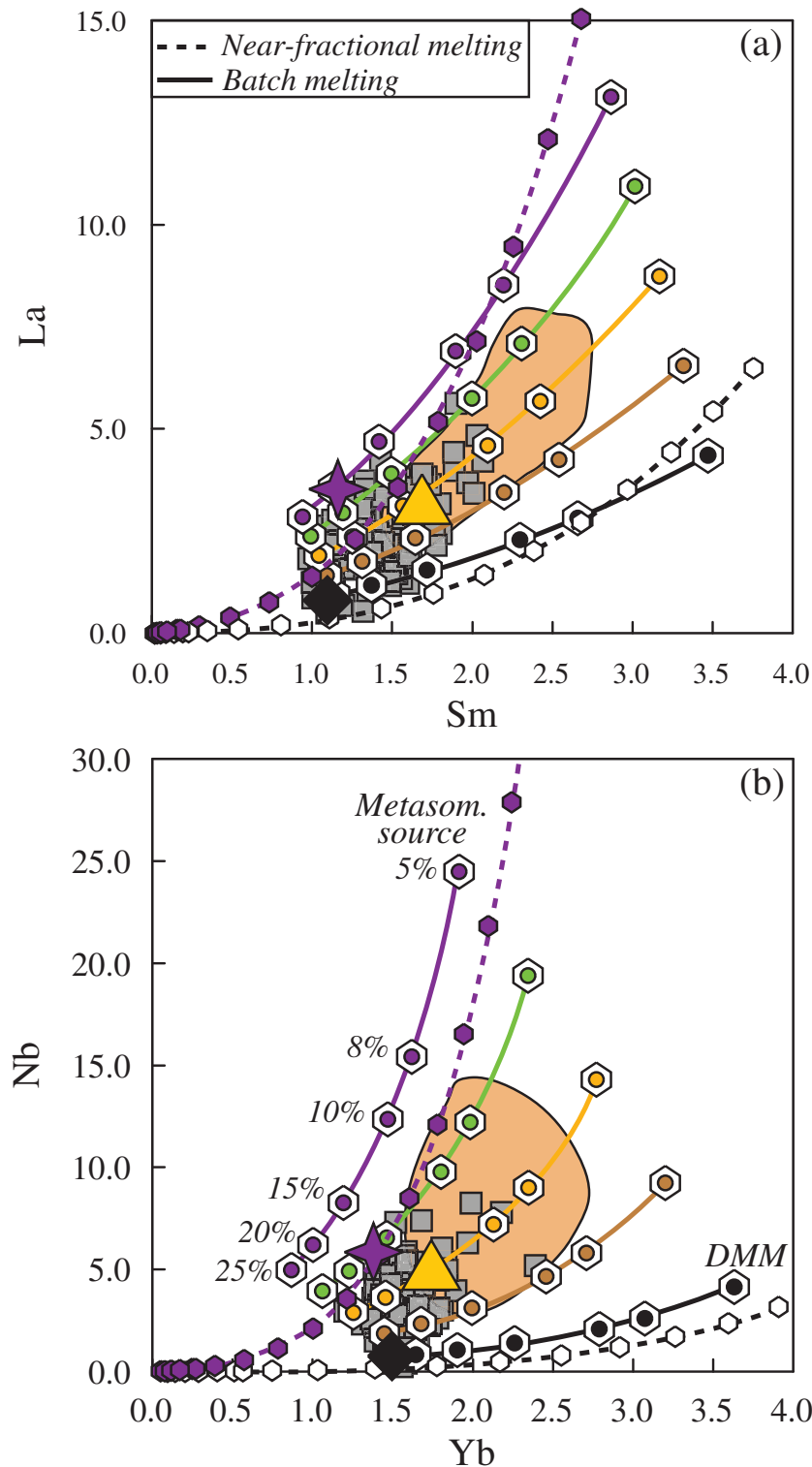


Fig. 14. (a) La vs Sm and (b) Nb vs Yb in high-Mg melt inclusions and low-Al lavas. The batch melting grid constructed by Gale *et al.* (in preparation) to explain the trace element and isotopic compositions of the FAMOUS lavas is illustrated here for an array of sources that are mixtures between two end-members—the metasomatized enriched source (Gale *et al.*, 2011) and the Salters & Stracke (2004) DMM. The sources contain 100%, 75%, 50%, 25% and 0% DMM respectively. These source mixtures are then melted to varying extents (5–25 wt %). Decompression near-fractional melting curves modeled with pHMELTS (with 2% of melt retained in the residue; as described in the text and previous figures) are indicated for the two end-member sources. The three large symbols (star, diamond and triangle) correspond to three melt inclusion compositions that can be tracked from plot (a) to (b) as they consistently record three different source compositions and melting extents. Similar to what is proposed for the lavas (Gale *et al.*, in preparation), most high-Mg melt inclusion compositions can be explained as pooled melts from various source compositions; they are, however, characterized by much higher melting extents. The most depleted high-Mg inclusions still require near-fractional melting. Lava compositions in equilibrium with $F_{0.0}$ are illustrated as compositional fields (Gale *et al.*, in preparation).

Table 4: Source compositions used for modeling of partial melting processes

| Source | DMM (Salters & Stracke) | Metasomatized source | Mixed source | Ultra-depleted source |
|--------------------------------|-------------------------|----------------------|--------------|-----------------------|
| SiO ₂ (wt %) | 44-85 | 44-71 | 44-71 | 44-91 |
| TiO ₂ | 0-08 | 0-13 | 3-98 | 0-04 |
| Al ₂ O ₃ | 3-41 | 3-98 | 0-1 | 2-38 |
| FeO* | 7-5 | 8-2 | 8-2 | 8-2 |
| MnO | 0-13 | 0-13 | 0-13 | 0-13 |
| MgO | 39 | 38-73 | 38-73 | 41-59 |
| CaO | 3-06 | 3-17 | 3-17 | 2-14 |
| Na ₂ O | 0-22 | 0-28 | 0-28 | 0-055 |
| K ₂ O | 0-01 | 0-006 | 0-57 | 0-006 |
| P ₂ O ₅ | 0-007 | 0-019 | 0-13 | 0-019 |
| Cr ₂ O ₃ | 0-39 | 0-57 | 0-006 | 0-39 |
| Rb (ppm) | 0-088 | 0-685 | 0-327 | 0-012 |
| Sr | 9-8 | 15-2 | 11-84 | 4-456 |
| Y | 4-07 | 1-88 | 3-194 | 3-971 |
| Zr | 7-94 | 5-48 | 6-956 | 3-948 |
| Nb | 0-21 | 1-24 | 0-622 | 0-039 |
| Ba | 1-2 | 8-072 | 3-95 | 0-139 |
| La | 0-234 | 0-706 | 0-423 | 0-07 |
| Ce | 0-772 | 1-473 | 1-05 | 0-283 |
| Nd | 0-713 | 0-85 | 0-768 | 0-421 |
| Sm | 0-27 | 0-22 | 0-27 | 0-199 |
| Eu | 0-107 | 0-084 | 0-107 | 0-092 |
| Gd | 0-395 | 0-288 | 0-395 | 0-363 |
| Tb | 0-075 | 0-049 | 0-062 | 0-073 |
| Dy | 0-531 | 0-326 | 0-5 | 0-549 |
| Ho | 0-122 | 0-069 | 0-11 | 0-131 |
| Er | 0-371 | 0-205 | 0-32 | 0-419 |
| Yb | 0-401 | 0-211 | 0-325 | 0-45 |
| Lu | 0-063 | 0-034 | 0-051 | 0-072 |
| Hf | 0-199 | 0-155 | 0-181 | 0-126 |
| Th | 0-0137 | 0-086 | 0-0426 | 0-002 |
| U | 0-0047 | 0-024 | 0-0124 | 0-0011 |

DMM composition is from Salters & Stracke (2004). The metasomatized source corresponds to the source fitted to explain the geochemistry of the Lucky Strike and Menez Gwen enriched lavas (Gale *et al.*, 2011). The mixed source composition corresponds to a composition of *c.* 60% DMM and 40% metasomatized source, with proportions selected to reproduce most of the high-Mg melt inclusion compositions. The depleted source corresponds to the residue of 4% of near-fractional melting (near-fractional melting with 2% of the melt retained in the residue) of an enriched Azores-like source in the garnet regime.

Azores hot spot source (Gale *et al.*, 2011), and a depleted mantle source, the Salters & Stracke (2004) DMM. These source mixtures are then batch melted to varying extents. The source is constrained by the isotope data, and the

extent of melting is constrained by the trace elements. This model is able to reproduce accurately the entire range of isotope and trace element variations in the low-Al lavas to remarkable precision [see also the concept of ‘dynamic source’ defined by Kamenetsky & Maas (2002) for a single MORB suite from Maquarie Island].

The success of the source heterogeneity model for the lavas raises the question of its applicability to the high-Mg melt inclusions. The Gale *et al.* (2011) model creates a ‘grid’ of predicted compositions based on source variation and extent of melting. Figure 14 displays similar grids on plots of La vs Sm and Nb vs Yb, with both lavas and high-Mg melt inclusions shown. The high-Mg inclusions overlap with the most depleted lavas, but extend to much lower abundances, suggesting a similar range of sources but overall higher mean extents of melting than the lavas. Notably, melt inclusions also record both lower and higher proportions of the enriched source than the lavas. Therefore a successful model for most of the high-Mg inclusions is an extension of the model for the lavas, with the melt inclusions sampling a greater diversity of sources, as would be expected.

What is unexpected is that the melt inclusions also sample higher extents of melting than the lavas. This was previously demonstrated by the trace element patterns presented in Fig. 6. The melt inclusion data are all at lower abundances than the lavas, and this fact remains true even when the inclusions and lavas are corrected to the same extent of fractionation, back-tracking the compositions of the lavas to be in equilibrium with Fo₉₀ olivine (as has been done for the lavas plotted in Figs 12–14).

It should be noted that the most depleted melt inclusions are not explained by this model. The very low Ba and Ba/La are even more depleted than DMM. These rare compositions require high-degree near-fractional melts as one contribution to the spectrum of high-Mg lavas. Most of the inclusions, however, are consistent with pooled melts from the same spectrum of source compositions required by the lavas. This model is testable by isotope measurements of melt inclusions, although this is currently beyond technical capability for these low-abundance samples.

There is one more intriguing aspect to the high extents of melting suggested by the high-Mg inclusions. A particularity of the melt inclusion compositions is the high CaO contents (i.e. higher CaO contents than in the lavas) and high CaO/Al₂O₃ (>0.9) in some inclusions. This major element characteristic is consistent with the conclusion that the melt inclusions are derived by high extents of melting from the top of the melting regime. As long as such melts are still formed when clinopyroxene is present in the residue, they will have the highest CaO contents of any melts within the melting regime. When an LLD is calculated using Petrolog from the high CaO/Al₂O₃ inclusion compositions, the sequence is olivine, olivine + cpx, then

olivine + cpx + plg, even at low P (1 bar). This sequence has also been observed in some FAMOUS lavas that display the same characteristic of high $\text{CaO}/\text{Al}_2\text{O}_3 > 0.86$ at 1 kbar. Also, LLDs calculated from experimental lherzolite melts of DMM1 and MM3 show the same difference in their crystallization sequence, depending on the starting $\text{CaO}/\text{Al}_2\text{O}_3$ of the melt. For example, an $F=2\%$ melt from DMM1 has a $\text{CaO}/\text{Al}_2\text{O}_3$ of 0.74 (Wasylenki *et al.*, 2003), and crystallizes olivine, olivine + plag, and olivine + plag + cpx at 1 kbar, as is classically observed in MORBs. However, an 11% melt with a $\text{CaO}/\text{Al}_2\text{O}_3$ of 0.96 crystallizes olivine–olivine + cpx–olivine + cpx + plag. The same difference is observed between a 7% melt of MM3 ($\text{CaO}/\text{Al}_2\text{O}_3=0.63$) and a 22% melt ($\text{CaO}/\text{Al}_2\text{O}_3=0.98$) (Baker *et al.*, 1995; Hirschmann *et al.*, 1998). The high- F experimental liquids from peridotite melting have CaO contents that are comparable with or higher than those of the high-Ca melt inclusions. Therefore, although insufficient correction for post-entrapment re-equilibration can result in higher CaO abundances, these observations suggest that the melt inclusion compositions may not be anomalous in their CaO content, and that the distinctive sequence of crystallization observed from the high-Ca inclusions is consistent with sequences obtained for both lavas and experimental melts that display similar high $\text{CaO}/\text{Al}_2\text{O}_3$ signatures. This signature supports high degrees of melting at the top of the melting column.

This possibility of clinopyroxene appearing before plagioclase on the liquidus permits the crystallization of high-Mg-number clinopyroxene, and may be an explanation for the origin of the high-Mg-number poikilitic clinopyroxenes reported by Lissenberg & Dick (2008). High-degree melts from the top of the melting regime have high-Mg-number cpx on the liquidus, which precipitates when these liquids cool and encounter lower crustal cumulates.

Origin of the parental melts for the high-Al melt inclusions

High-Al melt inclusions display distinctive trace element characteristics (i.e. ultra-depleted concentrations and low MREE/HREE ratios), which imply a different petrogenesis for these melts. A key line of evidence is shown in Fig. 15b, which illustrates that the offset in the low MREE/HREE melts towards higher Yb contents for a given Sm content cannot be reproduced by mixing of melts derived from a single melting column of a homogeneous mantle source. Another line of evidence is that Na_2O contents vary consistently with Yb contents; for a given TiO_2 content, Na_2O is generally higher in high-Al melt inclusions than in the rest of the inclusions (Electronic Appendix 4).

All of these characteristics—ultra-depleted values of incompatible elements, low MREE/HREE, and slightly high Na_2O —can be explained by melting of a source that

has undergone previous melting in the garnet stability field (Fig. 15). Residual garnet in the first melting event would retain the HREE preferentially, leading to a source with low MREE/HREE ratios; removal of the melt would also produce very low incompatible element contents and depleted incompatible element ratios. Na is characterized by an increase of the partition coefficient between clinopyroxene and melt with pressure (Blundy *et al.*, 1995). Melting in the garnet field therefore would also cause Na to be retained more in the residue than at lower pressure; when this residue melts again, Na concentrations would therefore be higher in the resultant melts.

The sequence of events involves a first step of deep melting of a garnet lherzolite; the solid residue then moves upward and melts in the spinel stability field to produce liquids with distinctively low MREE/HREE ratios. The extent of melting in the garnet regime necessary to obtain MREE/HREE ratios consistent with the melt inclusion data depends on the starting mantle composition; some melt retention is also necessary to prevent over-depleting the source. If an enriched Azores-type mantle is the starting composition (the most likely enriched mantle to start melting deep and be transported along the ridge), continuous melting in the garnet stability field with one step of melt removal ($F=4$ wt %) with 2 wt % of melt retained produces a possible source (see Table 4). This first melting of an enriched mantle in the garnet stability field strongly depletes incompatible trace element contents in the solid residue, fractionates highly incompatible element ratios such as Ba/La, Ba/Nb and Rb/Nb, and leads to low MREE/HREE because of retention of the HREE in garnet. The compositions of the most depleted high-Al melt inclusions with the lowest MREE/HREE ratios can then be reproduced by ~12–17% near-fractional melting of that residue in the spinel regime (Fig. 15). Our melting and source generation model for the high-Al, low MREE/HREE melts is similar to the concept of mantle preconditioning proposed by Pearce (2005), in which small fractions of melt, preferentially from enriched ‘plum’ components—here from the Azores plume material—are extracted at depth from the asthenosphere during its flow to the major site of magma generation.

It should be noted that this explanation does not account for the distinctive major element compositions of the high-Al inclusions, nor the positive Sr anomalies in some of them. As noted above, we attribute the high Al_2O_3 , low SiO_2 and positive Sr anomalies to reaction of primitive high-Al melts, produced as described in the previous paragraph, with troctolitic compositions in the lower crust. This interaction produces changes in major elements and trace elements such as Sr that are enriched in the plag-bearing cumulates, but does not change the MREE/HREE ratios (Gurenko & Sobolev, 2006). Although such assimilation can also lower incompatible elements (e.g.

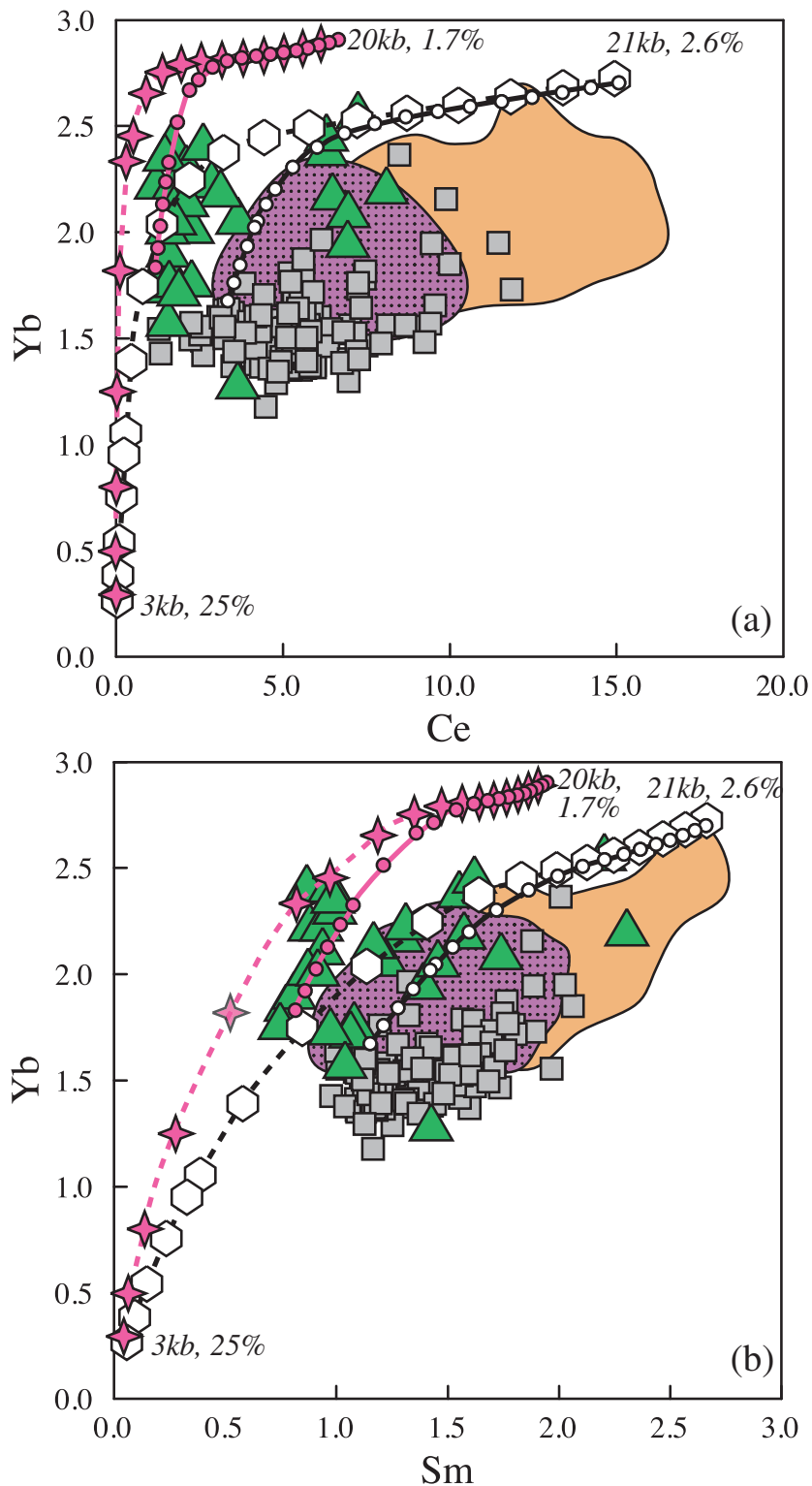


Fig. 15. (a) Yb vs Ce and (b) Yb vs Sm in high-Al melt inclusions. High-Mg melt inclusion compositions are plotted for comparison. A decompression melting curve from a depleted residue left after melting in the garnet stability field is shown for near-fractional instantaneous melts (stars; 2% melt retained) and pooled (filled circles) melts. The instantaneous near-fractional (hexagons; 2% melt retained) and pooled (open circles) melting curves for DMM (Salters & Stracke, 2004) are shown for comparison. Symbols on the melting curves represent 1 kbar decompression steps. (See text and Table 4 for the source compositions and details of melting modeling.) Lava compositions in equilibrium with F_{090} are indicated as compositional fields (Gale *et al.*, in preparation).

Danyushevsky *et al.*, 2004), this effect requires much larger extents of assimilation than can be accommodated by the elements that are most sensitive to this process (e.g. Sr, Ba). For this reason the ultra-depleted character of these inclusions must also be inherited from their parental magmas.

Implications for melt formation and segregation

The results of this study have significant implications for the scale and character of mantle sources beneath the FAMOUS segment, the pathways of melt to the surface, and the character of shallow mixing at the ridge axis.

As shown above, the diversity of high-Mg melt inclusions is best explained as a product of variable extents of melting of source regions with large magnitude variations in trace element composition. These results are consistent with the variations observed in the lavas, which demonstrate significant isotopic heterogeneity in the mantle beneath the FAMOUS segment (Gale *et al.*, in preparation). Isotopes and trace elements in the lavas correlate in ways that are entirely consistent with the model for the melt inclusions. This extensive heterogeneity still does not, however, account for the trace element characteristics of the high-Al melt inclusions and lavas, which require an additional source and process.

Although it is difficult to infer the scale of heterogeneity in the mantle source, there is information on the scale of heterogeneity in the erupted lavas. The high-Al, low MREE/HREE samples are mostly geographically restricted to Mount Pluto near the center of the FAMOUS segment, with the exception of samples CH31-D8 and CH31-D12 (Bougault & Hékinian, 1974), samples CYA74-30-32 and CYA74-30-34 from the northeastern flank of Mount Venus (Arcyana, 1977), all collected on the inner floor of the rift valley, and three samples located on the northern fracture zone (ARP74-14-31, ARP74-14-32 and ARP74-14-33). The volcanic cones of Mount Venus and Mount Pluto that constitute the inner floor of the FAMOUS axial valley consist mainly of picritic and olivine basalts and are thought to result from the most recent volcanism in the area (Bougault & Hékinian, 1974; Hékinian & Hoffert, 1975; Harpp & White, 1995). Even though some of the high-Al lavas are not located in the vicinity of Mount Pluto, almost all of them were collected on the inner floor of the rift valley and are therefore likely to be amongst the most recently erupted lavas. It therefore appears that high-Al, low MREE/HREE lavas result from a late stage of volcanism, erupting a new batch of magma that exhibits specific characteristics in major and trace elements. At the same time, the melt inclusions in these lavas consist of both the high-Al and high-Mg groups, raising the possibility that batches of both liquid compositions were present simultaneously.

The question of temporal variability is not easily resolved, because it is possible that ascending magma captures olivines from older liquids with a different composition. Although the question of temporal variation vs simultaneity cannot be resolved in detail, the fact remains that the entire spectrum of lava and inclusion compositions exists along an ~2 km wide swath of the rift valley floor. Volumes of single lava flows must be small, as indicated by the detailed mapping of lava compositions originally carried out by Bryan & Moore (1977). Therefore discrete melts that sample discrete mantle domains are able to arrive at the surface and produce small lava flows containing an even greater diversity of inclusion compositions. Mantle heterogeneities are 'small' (kilometer scale), and can be effectively preserved from mantle source to the liquid arriving at the surface. This is consistent with work by Kogiso *et al.* (2004) on diffusive equilibration of mantle heterogeneities that has shown that mantle domains as small as a few meters wide can retain and produce melts with distinctive geochemical signatures in a melting regime. Mixing of melts with distinctive trace element characteristics thus appears to be a shallow process, rather than an event that takes place in the mantle prior to ascent.

The offset in chemical composition between the melt inclusions and the lavas also has implications for the origin of the melt inclusions and the pathways of melt migration from depth to the surface. The central pieces of evidence are first that the melt inclusions are derived from greater extents of melting than the lavas, and second that the range in sources of the melt inclusions is slightly greater than but overall similar to that of the lavas.

One possible explanation for the first observation would be that only the more depleted lavas contain abundant olivine, and so the more depleted melt inclusions reflect a sampling bias caused by which samples were selected for melt inclusion study. This appears not to be the case for the following reasons. First, one of the samples selected was the most enriched sample in the segment, a true enriched (E)-MORB (NR-DR3). Notably, the olivines in this sample contain only depleted high-Mg inclusions (see Table 2). Second, within other samples, the average melt inclusion composition is more depleted than the lava composition (see the respective values of the La/Sm ratio in Table 2). The greater depletion of the high-Mg inclusions relative to the lavas thus appears to be a robust feature of the dataset. The challenge is then to understand this observation in the context of the ridge melting regime.

A possible explanation for these results comes from a consideration of the geometry of the melting regime, using the melting triangle and 'residual mantle column' (RMC) concepts presented by Langmuir *et al.* (1992), coupled with the proposal of melt extraction through high-porosity channels at the base of the lithosphere as

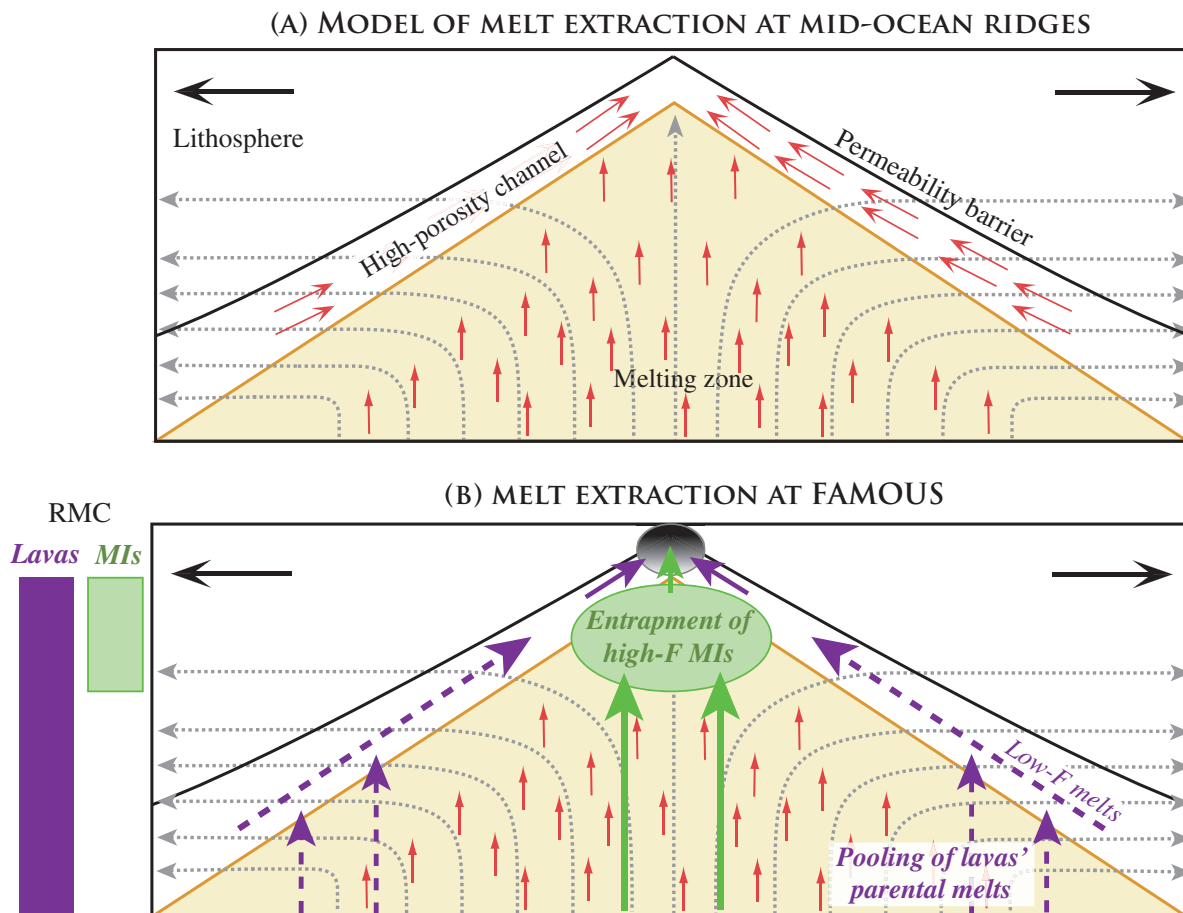


Fig. 16. Schematic illustrations of (a) the melt focusing model of melt channelling at mid-ocean ridges as proposed by Sparks & Parmentier (1991), Spiegelman (1993), Katz (2008) and Hebert & Montési (2010) (Fig. after Spiegelman, 1993 and Hebert & Montési, 2010), and (b) our model of melt extraction at FAMOUS. In the melt channelling model, melts are produced in the melting zone and rise buoyantly (small arrows) to the thermal boundary layer at the base of the lithosphere, where they crystallize and form a permeability barrier. A high-porosity channel develops along the base of the sloping lithosphere, allowing melt to flow toward the ridge axis. Gray dotted lines represent the solid flow streamlines. In our model, high-Mg melt inclusions are trapped at the top of the melting regime and preferentially record high-degree melts, whereas lavas are representative of the pooled melts that sample the whole melting region. The low-degree melts formed at the edges of the melting regime rise to the thermal boundary layer and then flow toward the ridge axis in the high-porosity channels, and are therefore not recorded in the melt inclusions. The corresponding residual mantle columns (RMC) are shown for the high-Mg melt inclusions and the lavas. The pooled melts at the top of the porosity channels entrain the primitive olivine crystals that enclose the high-Mg melt inclusions; they differentiate and react with the crust before their eruption at the surface.

proposed by, for example, Sparks & Parmentier (1991), Spiegelman (1993), Katz (2008) and Hebert & Montési (2010) (Fig. 16). In these models, melts produced in the melting zone rise buoyantly to the thermal boundary layer at the base of the lithosphere where they crystallize and form a permeability barrier. A high-porosity channel then develops along the base of the sloping lithosphere, allowing melt to flow diagonally upwards towards the ridge axis.

Although the melt inclusions record a very large diversity of melt compositions, the compositions are biased toward high-degree melts from the upper portions of the

melting column. Even inclusion compositions from more enriched sources in this region are derived by high extents of melting (Fig. 14). The lavas, on the other hand, seem to be pooled melts from the entire melting regime.

The implication of this result is that melts formed at the edge of the melting regime, produced at great depth, are transported along high-porosity channels at the top of the melting regime and arrive at the surface without having been trapped as olivine-hosted melt inclusions. Melts from the center of the melting regime, however, are formed over pressure intervals that extend all the way to the surface, and temperatures of melt formation and of olivine

saturation at shallow pressure are very close to one another. These melts may also form sills in the shallow mantle where melt inclusions may form. Whatever the exact physical cause, the data indicate that melt inclusions form preferentially from shallow melts formed at the top of melting regime.

In terms of the RMCs, the central columns represent the greatest extents of melting, forming only the topmost portions of the RMC. These liquids and their olivines are then mixed with the lower-degree melts from the edges of the melting regime that have had a physically separate transport to the surface. Mixing of both deep and shallow melts creates the range of erupted lavas. Lavas then reflect pooled melts from the entire melting regime; melt inclusions represent melts from the top of the melting regime (Fig. 16). Because melting is largely fractional, this also permits late-stage, highly depleted fractional melts from the top of the melting regime to be represented in the inclusion compositions.

All these results imply that a simple continuous melting column model, such as the one proposed for the FAMOUS lavas by Langmuir *et al.* (1977) and for the study of MAR melt inclusions by Sobolev & Shimizu (1993), cannot fully explain the diversity of melts erupted along the FAMOUS segment. Source heterogeneity is a critical factor, at least in this region, in creating the diversity of melt inclusion and lava compositions. Furthermore, the melt inclusions do not reflect the fractional melting products of the entire melting regime. Instead, inclusions preferentially sample the upper portions of the melting regime. Most melt inclusions are not fractional melts, but are pooled melts from the central portions of the melting regime.

The other surprising aspect of the data we report is the lack of correspondence between trace elements and major elements. For a decompression melting column model, we would expect lower SiO_2 and higher Al_2O_3 and FeO^* contents in the deep, trace element enriched, low-degree melts than in the high-degree melts generated at lower pressures. The most enriched melts of the high-Mg melt inclusions, however, are not characterized by lower SiO_2 than the more depleted high-Mg melt inclusions. In addition, the large differences in extents of melting and source compositions that are apparent from the trace elements are not evident in the rather subdued major element variations. It appears that the trace elements more directly reflect small-scale variations in the source and extent of melting, whereas the major elements are more able to reflect mean properties. This may be a consequence of melt re-equilibration at various pressures that would significantly modify the major element compositions but have little effect on trace element abundances and ratios. In addition, as we demonstrated for the high-Al inclusions, melt-rock reactions can generate significant changes in the

major element compositions of mantle melts, whereas the modifications to the trace elements are too small to erase the effects of melting and mantle source variability. The detailed relationship between major and trace element variations, however, poses many questions that remain to be fully explored.

In comparison with previous studies (e.g. Langmuir *et al.*, 1977; Shimizu, 1998; Laubier *et al.* 2007), our new view of the FAMOUS area from a combined lava and melt inclusion study reveals much greater detail and complexity. Source heterogeneity is a central feature of the diversity of magma compositions. Melt inclusions are not representative of the total range of parental magmas, and are instead biased towards high-degree melts from the top of the melting regime. Furthermore, although instantaneous fractional melts are occasionally present in melt inclusions, most of the inclusions represent pooled melts from the central columns of the melting regime. Major elements in melt inclusions and some lavas are also influenced by interaction between the ascending melts and the cumulate pile that must be traversed for the magmas to reach the surface.

CONCLUSIONS

Our study presents an extensive and currently unique major and trace element dataset for olivine-hosted melt inclusions from 14 samples from a single mid-ocean ridge segment, the FAMOUS segment of the Mid-Atlantic Ridge, which can be compared with an exhaustive study of lavas from every station in the segment (Gale *et al.*, in preparation). The study of multiple samples from a single ridge segment, and the comparison between lavas and melt inclusions, permits a new perspective on the processes involved in the formation of melt inclusions and how they relate to the erupted lavas. Our results can be summarized as follows.

- (1) Major element re-equilibration after melt entrapment in the host crystal has been recognized in some of the FAMOUS melt inclusions. Using the correlation between Yb and Fe observed in the lavas, corrections have been made to variable rather than constant Fe contents, avoiding the common correction to constant FeO that eliminates all initial variations.
- (2) Trace element concentrations in olivine-hosted melt inclusions are little affected by post-entrapment diffusion or olivine overgrowth. Melt inclusions extend the chemical variability observed in the lavas; they are generally more primitive and their incompatible element abundances are on average shifted towards lower values. High-Mg melt inclusions could constitute the potential parental melts of the lavas, but their Na_2O , TiO_2 and incompatible element contents

- are too low to generate the lava compositions by differentiation.
- (3) The FAMOUS melt inclusions form three discrete groups. High-Mg inclusions constitute melts little modified from their origin in the melting regime. Low-Al inclusions are mixtures of high-Mg melt inclusions with the lava compositions. High-Al melt inclusions have a distinct petrogenesis in terms of their major and trace elements.
 - (4) High-Al melt inclusions display major and trace element characteristics (high Al_2O_3 , low SiO_2 , low incompatible element concentrations) that have previously been reported for high-Al basalts in other mid-ocean ridge studies (Eason & Sinton, 2006; Lissenberg & Dick, 2008). Assimilation of plagioclase-bearing crustal material by the ascending melt can explain most of the major element characteristics of the high-Al melt inclusions and the positive Sr anomalies observed in some high-Al inclusions. Our results rule out high-pressure clinopyroxene fractionation as the process that generates high-Al melts. Trace elements in the FAMOUS high-Al inclusions still retain source characteristics, and require an early melt depletion event in the presence of garnet prior to a second melting event leading to the low MREE/HREE characteristic of the parental magmas.
 - (5) The high-Mg melt inclusions can be largely explained by different extents of partial melting of a heterogeneous source, consistent with results for the lavas (Gale *et al.*, in preparation). However, the melt inclusions are derived by greater extents of melting than the lavas. Most high-Mg inclusions appear to be pooled melts, but ultra-depleted high-Mg inclusions require an origin by fractional melting at the top of the melting regime.
 - (6) The contrast between lava and melt inclusion compositions can be understood in the context of the ridge melting regime. Lavas sample the entire melting regime, including low-degree melts from the wings of the melting regime that are transported to the surface along high-porosity channels. Melt inclusions come from the upper portions of the melting regime, where extents of melting are greater. Pooling of the low-degree melts not present in the melt inclusion population, with the high-degree melts sampled by the melt inclusions, leads to the erupted lava compositions.
 - (7) The melt inclusion results also suggest solutions to some long-standing enigmas of MORB petrogenesis. High-Al inclusions may bear the imprint of reaction with, and assimilation of, troctolite in the crust, and the same process may lead to the high-An plagioclase megacrysts that often occur in highly plagioclase-phyric MORB. The existence of high-degree melts from the top of the melting regime with high CaO/

Al_2O_3 may also explain the poikilitic high-Mg-number clinopyroxenes found in some oceanic gabbros.

- (8) Major and trace elements in the melt inclusions do not show a coherent story in terms of pressure and temperature of origin. This has to do in part with modifications at shallow levels, but also may reflect the fact that major elements are easily modified by re-equilibration during magma ascent, whereas trace elements preserve the signatures of source and extent of melting.

ACKNOWLEDGEMENTS

Thanks go to Michael Jercinovic at UMass for assistance with electron microprobe operations, and to Zhongxing Chen at Harvard University for his support with the early stages of LA-ICP-MS analyses. This paper benefited substantially from the invaluable comments by Vadim Kamenetsky, John Maclennan and Leonid Danyushevsky. We greatly appreciate the editorial handling by M. Wilson.

FUNDING

This work was supported by the National Science Foundation (OCE-0850442).

SUPPLEMENTARY DATA

Supplementary data for this paper are available at *Journal of Petrology* online.

REFERENCES

- ARCYANA, (1977). Rocks collected by bathyscaph and diving saucer in the FAMOUS area of the Mid-Atlantic Rift Valley: petrological diversity and structural setting. *Deep-Sea Research* **24**, 565–589.
- Asimow, P. D., Dixon, J. E. & Langmuir, C. H. (2004). A hydrous melting and fractionation model for mid-ocean ridge basalts: Application to the Mid-Atlantic Ridge near the Azores. *Geochemistry, Geophysics, Geosystems* **5**, doi:10.1029/2003GC000568.
- Baker, M. B., Hirschmann, M. M., Ghiorso, M. S. & Stolper, E. M. (1995). Compositions of near-solidus peridotite melts from experiments and thermodynamic calculations. *Nature* **375**, 308–311.
- Bédard, J. H., Hébert, R., Berclaz, A. & Varfalvy, V. (2000). Syntexis and the genesis of lower oceanic crust. In: Dilek, I., Moores, E., Elthon, D. & Nicolas, A. (eds), *Ophiolites and Oceanic Crust: New Insights from Field Studies and the Ocean Drilling Program*. Geological Society of America, 105–119.
- Blundy, J. D., Falloon, T. J., Wood, B. J. & Dalton, J. A. (1995). Sodium partitioning between clinopyroxene and silicate melts. *Journal of Geophysical Research* **100**, 15501–15515.
- Bougault, H. (1977). Evidence de la cristallisation fractionnée au niveau d'une ride médio-océanique: Co, Ni, Cr, FAMOUS, leg 37 du DSDP. *Bulletin de la Société Géologique de France* **7**, 1207–1212.
- Bougault, H. & Hékinian, R. (1974). Rift Valley in the Atlantic Ocean near 36°50'N: Petrology and geochemistry of basaltic rocks. *Earth and Planetary Science Letters* **24**, 249–261.

- Bryan, W. B. & Moore, J. G. (1977). Compositional variations of young basalts in Mid-Atlantic Ridge rift valley near lat 36°49'N. *Geological Society of America Bulletin* **88**, 556–570.
- Cherniak, D. J. (2010). REE diffusion in olivine. *American Mineralogist* **95**, 362–368.
- Collier, M. L. & Kelemen, P. B. (2010). The case for reactive crystallization at mid-ocean ridges. *Journal of Petrology* **51**, 1913–1940.
- Cottrell, E., Spiegelman, M. & Langmuir, C. H. (2002). Consequences of diffusive re-equilibration for the interpretation of melt inclusions. *Geochemistry, Geophysics, Geosystems* **3**, article number 2001GC000205.
- Danyushevsky, L. V. & Plechov, P. (2011). Petrology3: Integrated software for modeling crystallization processes. *Geochemistry, Geophysics, Geosystems* **12**, Q07021, doi:10.1029/2011GC003516.
- Danyushevsky, L. V., Della-Pasqua, F. N. & Sokolov, S. (2000). Re-equilibration of melt inclusions trapped by magnesian olivine phenocrysts from subduction-related magmas: petrological implications. *Contributions to Mineralogy and Petrology* **138**, 68–83.
- Danyushevsky, L. V., McNeill, A. W. & Sobolev, A. V. (2002a). Experimental and petrological studies of melt inclusions in phenocrysts from mantle-derived magmas: an overview of techniques, advantages and complications. *Chemical Geology* **183**, 5–24.
- Danyushevsky, L. V., Sokolov, S. & Falloon, T. J. (2002b). Melt inclusions in olivine phenocrysts: using diffusive re-equilibration to determine the cooling history of a crystal, with implications for the origin of olivine-phyric volcanic rocks. *Journal of Petrology* **43**, 1651–1671.
- Danyushevsky, L. V., Leslie, R. A. J., Crawford, A. J. & Durance, P. (2004). Melt inclusions in primitive olivine phenocrysts: the role of localized reaction processes in the origin of anomalous compositions. *Journal of Petrology* **45**, 2531–2553.
- Danyushevsky, L. V., Perfit, M. R., Eggins, S. M. & Falloon, T. J. (2003). Crustal origin for coupled ‘ultra-depleted’ and ‘plagioclase’ signatures in MORB olivine-hosted melt inclusions: evidence from the Siqueiros Transform Fault, East Pacific Rise. *Contributions to Mineralogy and Petrology* **144**, 619–637.
- de Hoog, J. C. M., Koestser, G. W., Bronto, S., Sriwana, T. & van Bergen, M. J. (2001). Sulfur and chlorine degassing from primitive arc magmas: temporal changes during the 1982–1983 eruptions of Galunggung (West Java, Indonesia). *Journal of Volcanology and Geothermal Research* **108**, 55–83.
- Dixon, J. E., Clague, D. A. & Stolper, E. (1991). Degassing history of water, sulphur and carbon in submarine lavas from Kilauea volcano, Hawaii. *Journal of Geology* **99**, 371–394.
- Drouin, M., Godard, M., Ildefonse, B., Bruguier, O. & Garrido, C. J. (2009). Geochemical and petrographic evidence for magmatic impregnation in the oceanic lithosphere at Atlantis Massif, Mid-Atlantic Ridge (IODP Hole U1309D, 30°N). *Chemical Geology* **264**, 71–88.
- Eason, D. & Sinton, J. (2006). Origin of high-Al N-MORB by fractional crystallization in the upper mantle beneath the Galapagos Spreading Center. *Earth and Planetary Science Letters* **252**, 423–436.
- Fisk, M. R. & Bence, A. E. (1980). Experimental crystallization of chrome spinel in FAMOUS basalt 527-1-1. *Earth and Planetary Science Letters* **48**, 111–123.
- Font, L., Murton, B. J., Roberts, S. & Tindle, A. G. (2007). Variations in melt productivity and melting conditions along SWIR (70°E–49°E): evidence from olivine-hosted and plagioclase-hosted melt inclusions. *Journal of Petrology* **48**, 1471–1494.
- Frezzotti, M.-L. (2001). Silicate–melt inclusions in magmatic rocks: application of petrology. *Lithos* **55**, 273–299.
- Gaetani, G. A. & Watson, E. B. (2000). Open system behavior of olivine-hosted melt inclusions. *Earth and Planetary Science Letters* **183**, 27–41.
- Gaetani, G. A. & Watson, E. B. (2002). Modeling the major-element evolution of olivine-hosted melt inclusions. *Chemical Geology* **183**, 25–41.
- Gale, A., Laubier, M., Escrig, S., Langmuir, C. H. & Jacobsen, S. B. (2009). Constraints on melting processes and ridge segmentation by new high-precision investigation of basalts from the FAMOUS segment, Mid-Atlantic Ridge. San Francisco, CA: American Geophysical Union, Fall Meeting 2009, Abstract V33C-2059.
- Gale, A., Escrig, S., Gier, E. J., Langmuir, C. H. & Goldstein, S. L. (2011). Enriched basalts at segment centers: The Lucky Strike (37°17'N) and Menez Gwen (37°50'N) segments of the Mid-Atlantic Ridge. *Geochemistry, Geophysics, Geosystems* **12**, doi:10.1029/2010GC003446.
- Grove, T. L., Kinzler, R. J. & Bryan, W. B. (1992). Fractionation of mid-ocean ridge basalt (MORB). In: Phipps Morgan, J., Blackman, D. K. & Sinton, J. M. (eds) *Mantle Flow and Melt Generation at Mid-Ocean Ridges*. American Geophysical Union, Geophysical Monograph **71**, 281–310.
- Gurenko, A. A. & Chaussidon, M. (1995). Enriched and depleted primitive melts in olivine from Icelandic tholeiites: Origin by continuous melting of a single mantle column. *Geochimica et Cosmochimica Acta* **59**, 2905–2917.
- Gurenko, A. A. & Sobolev, A. V. (2006). Crust–primitive magma interaction beneath neovolcanic rift zone of Iceland recorded in gabbro xenoliths from Midfell, SW Iceland. *Contributions to Mineralogy and Petrology* **151**, 495–520.
- Harpp, K. S. & White, W. M. (1995). Chapter five: Chemical zonation within the inner rift valley floor of the FAMOUS area, Mid-Atlantic Ridge: preliminary results. PhD thesis. Ithaca, NY: Cornell University.
- Hebert, L. B. & Montési, L. G. J. (2010). Generation of permeability barriers during melt extraction at mid-ocean ridges. *Geochemistry, Geophysics, Geosystems* **11**, article number QJ2008.
- Hékinian, R. & Hoffert, M. (1975). Rate of palagonitization and manganese coating on basaltic rocks from the rift valley in the Atlantic Ocean near 36°50'N. *Marine Geology* **19**, 91–109.
- Herzberg, C. (2004). Partial crystallization of mid-ocean ridge basalts in the crust and mantle. *Journal of Petrology* **45**, 2389–2405.
- Hirschmann, M. M., Baker, M. B. & Stolper, E. M. (1998). The effects of alkalis on the silica content of mantle-derived melts. *Geochimica et Cosmochimica Acta* **62**, 883–902.
- Jackson, M. G. & Hart, S. R. (2006). Strontium isotopes in melt inclusions from Samoan basalts: Implications for heterogeneity in the Samoan plume. *Earth and Planetary Science Letters* **245**, 260–277.
- Kamenetsky, V. (1996). Methodology for the study of melt inclusions in Cr-spinel, and implications for parental melts of MORB from FAMOUS area. *Earth and Planetary Science Letters* **142**, 479–486.
- Kamenetsky, V. & Crawford, A. J. (1998). Melt–peridotite reaction recorded in the chemistry of spinel and melt inclusions in basalt from 43°N, Mid-Atlantic Ridge. *Earth and Planetary Science Letters* **164**, 345–352.
- Kamenetsky, V. S. & Gurenko, A. A. (2007). Cryptic crustal contamination of MORB primitive melts recorded in olivine-hosted glass and mineral inclusions. *Contributions to Mineralogy and Petrology* **153**, 465–481.
- Kamenetsky, V. S. & Maas, R. (2002). Mantle–melt evolution (dynamic source) in the origin of a single MORB suite: a perspective from magnesian glasses of Macquarie Island. *Journal of Petrology* **43**, 1909–1922.

- Kamenetsky, V. S., Eggins, S. M., Crawford, A. J., Green, D. H., Gasparon, M. & Falloon, T. J. (1998). Calcic melt inclusions in primitive olivine at 43°N MAR: evidence for melt–rock reaction/melting involving clinopyroxene-rich lithologies during MORB generation. *Earth and Planetary Science Letters* **160**, 115–132.
- Katz, R. F. (2008). Magma dynamics with the enthalpy method: Benchmark solutions and magmatic focusing at MORs. *Journal of Petrology* **49**, 2099–2121.
- Kelemen, P. B., Shimizu, N. & Salters, V. J. M. (1995). Extraction of mid-ocean-ridge basalt from the upwelling mantle by focused flow of melt in dunite channels. *Nature* **375**, 747–753.
- Kent, A. J. R. (2008). Melt inclusions in basaltic and related volcanic rocks. In: Putirka, K. D. & Topley, F. J. I. (eds) *Minerals, Inclusions and Volcanic Processes. Mineralogical Society of America and Geochemical Society, Reviews in Mineralogy and Geochemistry* **69**, 273–331.
- Klein, E. M. & Langmuir, C. H. (1987). Global correlations of ocean ridge basalt chemistry with axial depth and crustal thickness. *Journal of Geophysical Research* **92**, 8089–8115.
- Kobayashi, K., Tanaka, R., Moriguti, T., Shimizu, K. & Nakamura, E. (2004). Lithium, boron, and lead isotope systematics of glass inclusions in olivines from Hawaiian lavas: evidence for recycled components in the Hawaiian plume. *Chemical Geology* **212**, 143–161.
- Kogiso, T., Hirschmann, M. M. & Reiners, P. W. (2004). Length scales of mantle heterogeneities and their relationship to ocean island basalt geochemistry. *Geochimica et Cosmochimica Acta* **68**, 345–360.
- Langmuir, C. H., Klein, E. M. & Plank, T. (1992). Petrological systematics of mid-ocean ridge basalts: constraints on melt generation beneath ocean ridges. In: Phipps Morgan, J., Blackman, D. K. & Sinton, J. M. (eds) *Mantle Flow and Melt Generation at Mid-Ocean Ridges. Geophysical Monograph, American Geophysical Union* **71**, 183–280.
- Langmuir, C. H., Bender, J. F., Bence, A. E., Hanson, G. N. & Taylor, S. R. (1977). Petrogenesis of basalts from the FAMOUS area: Mid-Atlantic Ridge. *Earth and Planetary Science Letters* **36**, 133–156.
- Laubier, M., Schiano, P., Doucelance, R., Ottolini, L. & Laporte, D. (2007). Olivine-hosted melt inclusions and melting processes beneath the FAMOUS zone (Mid-Atlantic Ridge). *Chemical Geology* **240**, 129–150.
- Le Roex, A. P., Erlank, A. J. & Needham, H. D. (1981). Geochemical and mineralogical evidence for the occurrence of at least three distinct magma types in the ‘Famous’ region. *Contributions to Mineralogy and Petrology* **77**, 24–37.
- le Roex, A. P., Frey, F. A. & Richardson, S. H. (1996). Petrogenesis of lavas from the AMAR Valley and Narrowgate region of the FAMOUS Valley, 36°–37°N on the Mid Atlantic Ridge. *Contributions to Mineralogy and Petrology* **124**, 167–184.
- Lissenberg, C. J. & Dick, H. J. B. (2008). Melt–rock reaction in the lower oceanic crust and its implications for the genesis of mid-ocean ridge basalt. *Earth and Planetary Science Letters* **271**, 311–325.
- Lowenstern, J. B. (1995). Applications of silicate-melt inclusions to the study of magmatic volatiles. In: Thompson, J. F. H. (ed.) *Magma, Fluids and Ore Deposits. Mineralogical Association of Canada, Short Courses* **23**, 71–100.
- MacLennan, J. (2008a). Concurrent mixing and cooling of melts under Iceland. *Journal of Petrology* **49**, 1931–1953.
- MacLennan, J. (2008b). Lead isotope variability in olivine-hosted melt inclusions from Iceland. *Geochimica et Cosmochimica Acta* **72**, 4159–4176.
- McDonough, W. F. & Sun, S.-s. (1995). The composition of the Earth. *Chemical Geology* **120**, 223–253.
- Metrich, N. & Rutherford, M. J. (1992). Experimental study of chlorine behavior in hydrous silicic melts. *Geochimica et Cosmochimica Acta* **56**, 607–616.
- Nielsen, R. L., Crum, J., Bourgeois, R., Hascall, K., Forsythe, L. M., Fisk, M. R. & Christie, D. M. (1995). Melt inclusions in high-An plagioclase from the Gorda Ridge: an example of the local diversity of MORB parent magmas. *Contributions to Mineralogy and Petrology* **122**, 34–50.
- Norman, M. D., Garcia, M. O., Kamenetsky, V. S. & Nielsen, R. L. (2002). Olivine-hosted melt inclusions in Hawaiian picrites: equilibration melting, and plume source characteristics. *Chemical Geology* **183**, 143–168.
- Oskarsson, N., Sigvaldason, G. E. & Steinthorsson, S. (1982). A dynamic model of rift zone petrogenesis and the regional petrology of Iceland. *Journal of Petrology* **23**, 28–74.
- Pearce, J. A. (2005). Mantle preconditioning by melt extraction during flow: Theory and petrogenetic implications. *Journal of Petrology* **2005**, 973–997.
- Qin, Z., Lu, F. & Anderson, A. T. J. (1992). Diffusive reequilibration of melt and fluid inclusions. *American Mineralogist* **77**, 565–576.
- Roedder, E. (1979). Origin and significance of magmatic inclusions. *Bulletin de Minéralogie* **102**, 487–510.
- Ryan, W. B. F., Carbotte, S. M., Coplan, J. O., O’Hara, S., Melkonian, A., Arko, R., Weissel, R. A., Ferrini, V., Goodwillie, A., Nitsche, F., Bonczkowski, J. & Zemsky, R. (2009). Global Multi Resolution Topography synthesis. *Geochemistry Geophysics Geosystems* **10**, Q03014, doi:10.1029/2008GC002332.
- Saal, A. E., Hart, S. R., Shimizu, N., Hauri, E. H. & Layne, G. D. (1998). Pb isotopic variability in melt inclusions from oceanic island basalts, Polynesia. *Science* **282**, 1481–1484.
- Saal, A. E., Hart, S. R., Shimizu, N., Hauri, E. H., Layne, G. D. & Eiler, J. M. (2005). Pb isotopic variability in melt inclusions from the EMI–EMII–HIMU mantle end-members and the role of the oceanic lithosphere. *Earth and Planetary Science Letters* **240**, 605–620.
- Salters, V. J. & Stracke, A. (2004). Composition of the depleted mantle. *Geochemistry, Geophysics, Geosystems* **5**, 2003GC000597.
- Schiano, P. (2003). Primitive mantle magmas recorded as silicate melt inclusions in igneous minerals. *Earth-Science Reviews* **63**, 121–144.
- Shaw, A. M., Behn, M. D., Humphris, S. E., Sohn, R. A. & Gregg, P. M. (2010). Deep pooling of low degree melts and volatile fluxes at the 85°E segment of the Gakkel Ridge: Evidence from olivine-hosted melt inclusions and glasses. *Earth and Planetary Science Letters* **289**, 311–322.
- Shimizu, N. (1998). The geochemistry of olivine-hosted melt inclusions in a FAMOUS basalt ALV519-4-1. *Physics of the Earth and Planetary Interiors* **107**, 183–201.
- Slater, L., McKenzie, D., Grönvold, K. & Shimizu, N. (2001). Melt generation and movement beneath Theistareykir, NE Iceland. *Journal of Petrology* **42**, 321–354.
- Smith, P. M. & Asimow, P. D. (2005). Adiabatic: A new public front-end to the MELTS, pMELTS, and pHMELTS models. *Geochemistry, Geophysics, Geosystems* **6**, article number Q02004.
- Sobolev, A. V. (1996). Melt inclusions in minerals as a source of principal petrological information. *Petrology* **4**, 209–220.
- Sobolev, A. V. & Kostyuk, V. P. (1975). Magmatic crystallization based on a study of melt inclusions. *Fluid Inclusion Research* **9**, 182–253.
- Sobolev, A. & Nikogosian, I. K. (1994). Petrology of long-lived mantle plume magmatism: Hawaii, Pacific, and Réunion Island, Indian Ocean. *Petrology* **2**, 131–168.
- Sobolev, A. V. & Shimizu, N. (1993). Ultra-depleted primary melt included in an olivine from the Mid-Atlantic Ridge. *Nature* **363**, 151–154.

- Sobolev, A. V., Hofmann, A. W. & Nikogosian, I. K. (2000). Recycled oceanic crust observed in 'ghost plagioclase' within the source of Mauna Loa lavas. *Nature* **404**, 986–989.
- Sours-Page, R., Johnson, K. T. M., Nielsen, R. L. & Karsten, J. L. (1999). Local and regional variation of MORB parent magmas: evidence from melt inclusions from the Endeavour Segment of the Juan de Fuca Ridge. *Contributions to Mineralogy and Petrology* **134**, 342–363.
- Sours-Page, R., Nielsen, R. L. & Batiza, R. (2002). Melt inclusions as indicators of parental magma diversity on the northern East Pacific Rise. *Chemical Geology* **183**, 237–261.
- Spandler, C. & O'Neill, H. S. C. (2010). Diffusion and partition coefficients of minor and trace elements in San Carlos olivine at 1,300°C with some geochemical implications. *Contributions to Mineralogy and Petrology* **159**, 791–818.
- Spandler, C., O'Neill, H. S. C. & Kamenetsky, V. S. (2007). Survival times of anomalous melt inclusions from element diffusion in olivine and chromite. *Nature* **447**, 303–306.
- Sparks, D. W. & Parmentier, E. M. (1991). Melt extraction from the mantle beneath spreading centers. *Earth and Planetary Science Letters* **105**, 368–377.
- Spiegelman, M. (1993). Physics of melt extraction: theory, implications and applications. *Philosophical Transactions of the Royal Society of London, Series A* **342**, 23–41.
- Spiegelman, M. & Kelemen, P. B. (2003). Extreme chemical variability as a consequence of channelized melt transport. *Geochemistry, Geophysics, Geosystems* **4**, 2002GC000336.
- Spiegelman, M., Kelemen, P. B. & Aharonov, E. (2001). Causes and consequences of flow organization during melt transport: The reaction infiltration instability in compactible media. *Journal of Geophysical Research* **106**, 2061–2077.
- Stakes, D. S., Shervais, J. W. & Hopson, C. A. (1984). The volcanic-tectonic cycle of the Famous and Amar Valleys, Mid-Atlantic Ridge (36°47'N)—evidence from basalt glass and phenocryst compositional variations for a steady-state magma chamber beneath the valley midsections, Amar-3. *Journal of Geophysical Research* **89**, 6995–7028.
- Thordarson, T., Self, S., Oskarsson, N. & Huselboch, T. (1996). Sulfur, chlorine and fluorine degassing and atmospheric loading by the 1783–1784 AD Laki (Skaftar Fires) eruption in Iceland. *Bulletin of Volcanology* **58**, 205–225.
- Thorner, C. R., Sherrod, D. R., Siems, D. F., Heliker, C. C., Meeker, G. P., Oscarson, R. L. & Kauahikaua, J. P. (2002). *Whole-rock and glass major-element geochemistry of Kilauea volcano, Hawaii, near vent eruptive products: September 1994 through September 2001. US Geological Society Open-File Report*, pp. 02–7.
- Toplis, M. J. (2005). The thermodynamics of iron and magnesium partitioning between olivine and liquid: criteria for assessing and predicting equilibrium in natural and experimental systems. *Contributions to Mineralogy and Petrology* **149**, 22–39.
- Van Orman, J. A., Grove, T. L. & Shimizu, N. (2002). Diffusive fractionation of trace elements during production and transport of melt in Earth's upper mantle. *Earth and Planetary Science Letters* **198**, 93–112.
- Villiger, S., Müntener, O. & Ulmer, P. (2007). Crystallization pressures of mid-ocean ridge basalts derived from major element variations of glasses from equilibrium and fractional crystallization experiments. *Journal of Geophysical Research* **112**, B01202, doi:10.1029/2006JB004342.
- Wasylenki, L. E., Baker, M. B., Kent, A. J. R. & Stolper, E. M. (2003). Near-solidus melting of the shallow upper mantle: partial melting experiments on depleted peridotite. *Journal of Petrology* **44**, 1163–1191.
- Workman, R. K. & Hart, S. R. (2005). Major and trace element composition of the depleted MORB mantle (DMM). *Earth and Planetary Science Letters* **231**, 53–72.
- Yurimoto, H., Kogiso, T., Abe, K., Barszczus, H. G., Utsunomiya, A. & Maruyama, S. (2004). Lead isotopic compositions in olivine-hosted melt inclusions from HIMU basalts and possible link to sulfide components. *Physics of the Earth and Planetary Interiors* **146**, 231–242.